AD-A070 486 MARYLAND UNIV COLLEGE PARK DEPT OF PHYSICS AND ASTRONOMY F/G 20/5
SELF-CONSISTENT THEORY OF CYCLOTRON MASER INSTABILITY FOR INTEN--ETC(U)
1978 H UHM, R C DAVIDSON, K R CHU N00014-75-C-0309
UNCLASSIFIED PUB-78-126 NL

| OF |
AD
A070486

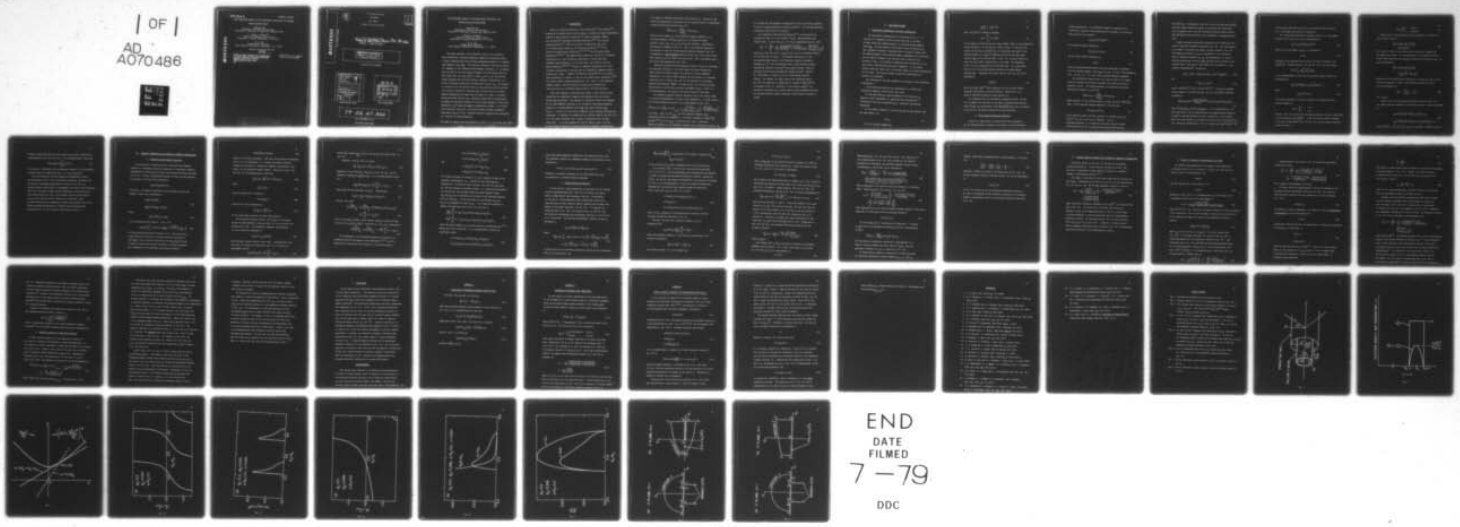

END
DATE
FILMED
7-79
DDC

PREPRINT #801P001

SELF-CONSISTENT THEORY OF CYCLOTRON MASER INSTABILITY FOR INTENSE HOLLOW ELECTRON BEAMS

Hwan-sup Uhm
Department of Physics and Astronomy
University of Maryland, College Park, Maryland 20742

Ronald C. Davidson*
Division of Magnetic Fusion Energy
Department of Energy, Washington, D. C. 20545

K. R. Chu
Plasma Physics Division
Naval Research Laboratory, Washington, D. C. 20375

Physics Publication #78-126

1978

Work on this report was supported by ONR Contract N00014-75-C-0309 and/or N00014-67-A-0239 monitored by NRL 6702.
02.

DDC PROCESSING DATA

PHOTOGRAPH

THIS SHEET

RETURN TO DDA-2 FOR FILE

II
LEVEL

1
INVENTORY

AD A070486
DDC ACCESSION NUMBER

Preprint 80IP001, Physics Pub. 78-126
DOCUMENT IDENTIFICATION

DISTRIBUTION STATEMENT A
Approved for public release;
Distribution Unlimited

DISTRIBUTION STATEMENT

Accession For
NTIS GRA&I
DDC TAB
Unannounced
Justification
By
Distribution/
Availability Codes
Dist. | Avail and/or special
A

DISTRIBUTION STAMP

DDC
RECEIVED
JUN 28 1979
D

DATE ACCESSIONED

79 06 27 322

DATE RECEIVED IN DDC

PHOTOGRAPH THIS SHEET

RETURN TO DDA-2

SELF-CONSISTENT THEORY OF CYCLOTRON MASER INSTABILITY FOR INTENSE HOLLOW ELECTRON BEAMS

Hwan-sup Uhm
Department of Physics and Astronomy
University of Maryland, College Park, Maryland 20742

Ronald C. Davidson*
Division of Magnetic Fusion Energy
Department of Energy, Washington, D. C. 20545

K. R. Chu
Plasma Physics Division
Naval Research Laboratory, Washington, D. C. 20375

This paper develops a self-consistent theory of the cyclotron maser instability, assuming azimuthally symmetric perturbations about a slowly rotating hollow electron beam propagating parallel to a uniform axial magnetic field $B_0\hat{e}_z$. The stability analysis is carried out within the framework of the linearized Vlasov-Maxwell equations. It is assumed that the beam is thin with radial thickness (2a) much smaller than the beam radius (R_0), and that $\omega_p^2/\omega_c^2 \ll 1$, where ω_p and ω_c are the electron plasma frequency and electron cyclotron frequency, respectively, in a frame of reference moving with the beam axial velocity $c\beta_b$. The analysis is carried out for the specific choice of equilibrium electron distribution function in which all electrons have the same value of canonical angular momentum and the same value of energy in a frame of reference moving with axial velocity $c\beta_b$. Stability properties are investigated including the important influence of finite radial geometry, finite beam temperature, and transverse magnetic perturbations ($\delta B \neq 0$). It is shown that instability exists for a very narrow range of axial wavenumbers satisfying $|k-\beta_b\omega/c| \ll 1/R_0$. Detailed stability properties are calculated for a variety of system parameters.

*On leave of absence from the University of Maryland, College Park, Md. 20742

I. INTRODUCTION

There is a growing literature on the equilibrium[1-4] and stability[5-18] properties of intense hollow electron beams, including the recent experimental studies of basic stability properties,[19] plasma confinement schemes such as Astron,[20] high-power microwave generation,[21-25] and electron ring accelerators.[25] Three of the basic instabilities that occur in a hollow electron beam are the diocotron instability,[5,6,19] the electron cyclotron maser instability,[8-11,21-24] and the negative-mass instability.[12-18,25] The negative-mass instability, which is an important instability for a fast rotational equilibrium, is associated with azimuthal charge bunching. On the other hand, the electron cyclotron maser instability,[8-11,21-24] which is a dominant instability for a slow rotational equilibrium, is present even for azimuthally symmetric perturbations with $\partial/\partial\theta=0$. However, the physical mechanism[9] for the cyclotron maser instability is similar to that for the negative-mass instability,[14-18] with radial charge clumping dominating for $\ell=0$. Here ℓ is the azimuthal harmonic number. The free energy for driving the instability is associated with the transverse energy spread of the beam electrons.

This paper develops a self-consistent theory of the cyclotron maser instability for azimuthally symmetric perturbations about an intense hollow beam equilibrium. The analysis is carried out within the framework of the Vlasov-Maxwell equations for an infinitely long beam propagating parallel to a uniform magnetic field $B_0\hat{e}_z$ with axial velocity $V_b\hat{e}_z$ (Fig. 1). The positive ions form an immobile ($m_i\to\infty$) partially neutralizing background. In addition, we assume that the electron beam is thin [Eq. (1)], i.e., the radial thickness (2a) is small in comparison with the mean radius (R_0). It is also assumed that $\omega_p^2<<\omega_c^2$, where ω_p and ω_c are the electron plasma frequency and electron cyclotron frequency, respectively,

in a frame of reference moving with axial velocity V_b. Equilibrium and stability properties are calculated for the specific choice of equilibrium electron distribution function [Eq. (8)],

$$f_e^0(H,P_\theta,p_z) = \frac{n_0 R_0}{2\pi m\gamma_b^2\gamma_0}\,\delta(U)\,\delta(P_\theta-P_0) \ ,$$

where H is the energy, P_θ is the canonical angular momentum, p_z is the axial momentum, $U\equiv H-\beta_b cp_z-\gamma_0 mc^2/\gamma_b$ is an effective energy variable, and n_0, R_0, γ_0, γ_b, β_b and P_0 are constants. Equilibrium properties are examined in Sec. II. One of the important features of the analysis is that the equilibrium distribution function in Eq. (8) corresponds to a sharp-boundary density profile [Eq. (17)], with uniform axial velocity over the beam cross section [Eq. (18)], and nonzero axial and radial beam temperatures [Eq. (21)].

Stability properties are investigated in Secs. III and IV, including the important influence of (a) finite axial and radial temperature, which limits the unstable range of k-values to a narrow bandwidth (Appendix C), (b) finite radial geometry and the presence of a grounded conducting wall at radius $r=R_c$, and (c) the influence of transverse magnetic perturbations ($\delta B_\theta \neq 0$). As shown in Sec. III, the most unstable perturbation is the TE mode with axial wavenumber $k\simeq\beta_b\omega/c$. Here ω is the eigenfrequency, and $c\beta_b\equiv V_b$ is the axial velocity of the beam.

The stability analysis predicts instability for a very narrow range of k values corresponding to $|kc-\beta_b\omega|\ll c/R_0$ (Appendix C). In this context, the TE mode dispersion relation can be approximated by [Eq. (71)]

$$\hat{p}^2(\hat{b}_-+\hat{b}_+)+(\omega-\omega_0)\left[\frac{d}{d\omega}\,(b_-+b_+)\right]_{\omega_0,k_0} = \frac{\nu(\omega-k_0V_b)}{\gamma_b\gamma_0R_0^2(\omega-k_0V_b-\omega_c/\gamma_b)}\left[1-\frac{\beta_0^2(\omega-k_0V_b)}{3(\omega-k_0V_b-\omega_c/\gamma_b)}\right] \ ,$$

for $kc\simeq\beta_b\omega$. Here, $\hat{b}_\pm=[b_\pm]_{\omega_0,k_0}$ are the normalized magnetic wave admittances defined in Appendix B, ν is Budker's parameter, $\hat{p}^2=\omega_0^2/c^2-k_0^2$, $\beta_0\equiv(\gamma_0^2-1)^{1/2}/\gamma_0$, and (ω_0,k_0) is defined in Eq. (66). A detailed numerical analysis of the dispersion relation (71) is carried out in Sec. IV.

It is found that the geometric configuration ($\hat{b}_-+\hat{b}_+$) and electron density (ν) have a strong influence of stability behavior. For low beam densities, instability exists only for $(\hat{b}_-+\hat{b}_+)\geq 0$.

As a comparison with previous analyses,[21] it is instructive to consider the limit of a very tenuous ($\nu/\gamma_0 \to 0$), infinitesimally thin ($a/R_0 \to 0$) beam. In this case, Eq. (71) can be approximated by [Eq. (69)]

$$\frac{\omega^2}{c^2} - k^2 - \frac{\alpha_{0n}^2}{R_c^2} = \frac{2\nu}{\gamma_0\gamma_b}\left[\frac{J_1(\alpha_{0n}R_0/R_c)}{R_c J_2(\alpha_{0n})}\right]^2\left[\frac{(\omega-kV_b)}{(\omega-kV_b-\omega_c/\gamma_b)} - \frac{\beta_0^2(\omega-kV_b)^2}{3(\omega-kV_b-\omega_c/\gamma_b)^2}\right]$$

where α_{0n} is the nth root of $J_1(\alpha_{0n})=0$ and $J_\ell(x)$ is the Bessel function of the first kind of order ℓ. The general features of Eq. (69) are qualitatively similar to the dispersion relation obtained by Friedman et al.[21] for perturbations about a self-consistent Vlasov equilibrium, $f_e^0 = \text{const.}\times\delta(H_\perp-\gamma_0 mc^2)\delta(p_z-\gamma_b m\beta_b c)\delta(P_\theta-P_0)$, where all electrons have the same perpendicular energy $H_\perp=\gamma_0 mc^2$. However, Eq. (69) differs in detail as do the corresponding stability results. For example, the final term on the right-hand side of Eq. (69) is proportional to $\beta_0^2(\omega-kV_b)^2/3$, instead of $\beta_0^2(\omega^2-k^2c^2)/2$ as obtained in Ref. 21. Moreover, in the previous study,[21] the system can be unstable for a broad range of axial wavenumbers whereas the present stability analysis predicts a narrow band of unstable k-values.

II. EQUILIBRIUM THEORY

A. Equilibrium Configuration and Basic Assumptions

The equilibrium configuration is illustrated in Fig. 1. It consists of a nonneutral hollow electron beam that is infinite in axial extent and aligned parallel to a uniform applied magnetic field $B_0\hat{e}_z$. The mean radius of the electron beam is denoted by R_0 and a grounded cylindrical conducting wall is located at radius $r=R_c$. The applied magnetic field provides radial confinement of the electrons, and the radial thickness of the electron beam is denoted by 2a. As shown in Fig. 1, we introduce cylindrical polar coordinates (r,θ,z) with z-axis coinciding with the axis of symmetry; r is the radial distance from the z-axis, and θ is the polar angle in a plane perpendicular to the z-axis. The electron charge is partially neutralized by a positive ion background.

The following are the main assumptions pertaining to the equilibrium configuration:

(a) Equilibrium properties are independent of z ($\partial/\partial z=0$) and azimuthally symmetric ($\partial/\partial\theta=0$) about the z-axis.

(b) The mean canonical angular momentum of the electrons is negative, which corresponds to a slow rotational equilibrium.[4,6] The positive ions form an immobile ($m_i\to\infty$), partially neutralizing background.

(c) The radial thickness of the electron beam is much smaller than the beam radius, i.e.,

$$a \ll R_0 . \tag{1}$$

(d) It is further assumed that

$$\frac{\nu}{\gamma_0}\frac{a}{R_0} << (\gamma_0^2-1)/\gamma_0^2 , \tag{2}$$

where $\nu=N_e e^2/mc^2$ is Budker's parameter,

$$N_e=2\pi \int_{R_1}^{R_2} dr\, r\, n_e^0(r) \tag{3}$$

is the number of electrons per unit axial length, $n_e^0(r)$ is the equilibrium electron density, c is the speed of light in vacuo, -e and m are the charge and rest mass, respectively, of an electron, and $\gamma_0 mc^2$ is the electron energy in a frame of reference moving with the mean axial velocity $V_b\hat{e}_z$ of the electron beam. In Eq. (3), R_1 and R_2 denote the inner and outer radii, respectively, of the beam. The inequality in Eq. (2) can be expressed in an alternate form. For a thin beam, from Eq. (3), the average electron density n_0 is approximately $n_0 \simeq N_e/(4\pi R_0 a)$. Combining this result with Eq. (16), Eq. (2) can be expressed as

$$\omega_p^2/\omega_c^2 << 1 \tag{4}$$

where $\omega_p=(4\pi n_0 e^2/\gamma_0 m)^{1/2}$ and $\omega_c=eB_0/\gamma_0 mc$ are the electron plasma frequency and electron cyclotron frequency, respectively, in a frame of reference moving with axial velocity V_b.

(e) Consistent with the low-density assumption in Eqs. (2) and (4), we neglect the influence of the small equilibrium self-electric field $E_r^s(r)\hat{e}_r$ and self-magnetic field $B_\theta^s(r)\hat{e}_\theta+B_z^s(r)\hat{e}_z$ that are produced by the lack of equilibrium charge and current neutrality.

B. Hollow Beam Equilibrium Properties

Central to a description of steady-state Vlasov equilibria are the single-particle constants of the motion in the equilibrium

field configuration. For azimuthally symmetric equilibria with $\partial/\partial\theta=0=\partial/\partial z$, there are three single-particle constants of the motion. These are the total energy H,

$$H=\gamma mc^2=(m^2c^4+c^2\underset{\sim}{p}^2)^{1/2} , \tag{5}$$

the canonical angular momentum P_θ,

$$P_\theta=r[p_\theta-(e/2c)rB_0] , \tag{6}$$

and the axial canonical momentum P_z,

$$P_z=p_z , \tag{7}$$

where the equilibrium-self-fields have been neglected in comparison with the external magnetic field $B_0\hat{\underset{\sim}{e}}_z$ [see Eqs. (2) and (4) and Assumption (e)]. In Eqs. (5) - (7), lower case $\underset{\sim}{p}$ denotes mechanical momentum.

Any distribution function that is a function only of the single-particle constants of the motion satisfies the steady-state Vlasov equation ($\partial/\partial t=0$). For present purposes, we assume an equilibrium distribution function of the form,[4]

$$f_e^0(H,P_\theta,P_z) = \frac{n_0R_0}{2\pi m\gamma_b^2\gamma_0}\,\delta(U)\delta(P_\theta-P_0) , \tag{8}$$

where n_0=const. is the electron density at $r=R_0$, $P_0\equiv-(e/2c)(R_0^2-a^2)B_0$= const. is the canonical angular momentum of the electrons,

$$U=H-\beta_b cp_z-\gamma_0mc^2/\gamma_b \tag{9}$$

is an effective energy variable, β_b=const. is defined by $\beta_b=V_b/c=(\gamma_b^2-1)^{1/2}/\gamma_b$, and γ_0 and γ_b are constants. In the subsequent analysis, it is shown that the axial velocity profile associated with Eq. (8) is uniform over the beam cross-section,

with $V_z^0(r)=\beta_b c$. Furthermore, since all of the electrons have the same canonical angular momentum $P_\theta=P_0\neq 0$, no electrons pass through the axis of symmetry (r=0), and the equilibrium electron density profile $n_e^0(r)=\int d^3p f_e^0$ calculated from Eq. (8) corresponds to a hollow electron beam.

Several pertinent equilibrium properties can be deduced for the class of thin-beam equilibria described by Eq. (8). For this purpose, it is useful to transform the energy variable U defined in Eq. (9) from momentum variables (p_r,p_θ,p_z) appropriate to the laboratory frame to momentum variables (p_r', p_θ', p_z') appropriate to a frame of reference moving with velocity $\beta_b c\hat{e}_z$ (the mean axial velocity of the electron beam). Here $\hat{e}_z$ is a unit vector in the z-direction. The relevant transformation[4] is given by

$$p_r=p_r',\ p_\theta=p_\theta',\ p_z=\gamma_b p_z'+\gamma_b\gamma'm\beta_b c,\ \gamma=\gamma_b(\gamma'+\beta_b p_z'/mc)\ , \tag{10}$$

and

$$U=\frac{1}{\gamma_b}(\gamma'-\gamma_0)mc^2\ , \tag{11}$$

where $\gamma=(1+p_r^2/m^2c^2)^{1/2}$ and $\gamma'=(1+p_r'^2/m^2c^2)^{1/2}$. After some straightforward algebra it follows from Eqs. (8)-(11) that $f_e^0 d^3p$ transforms according to

$$f_e^0(H,P_\theta,P_z)d^3p=\frac{n_0R_0(\gamma'+\beta_b p_z'/mc)}{2\pi m\gamma_0\gamma'}\,\delta(\gamma'mc^2-\gamma_0mc^2)\delta(P_\theta'-P_0)d^3p'\ , \tag{12}$$

where $d^3p=dp_r dp_\theta dp_z$ and $d^3p'=dp_r' dp_\theta' dp_z'$. It is evident from Eq. (12) that γ_0mc^2=const. can be identified with the total electron energy in a frame of reference moving with axial velocity $\beta_b c$. On the other hand, since the constant γ_b is defined in terms of β_b by $\beta_b=(\gamma_b^2-1)^{1/2}/\gamma_b$ [cf., discussion following Eq. (9)], it follows that $\gamma_b mc^2=(1-\beta_b^2)^{-1/2}mc^2$

is the energy associated solely with the directed axial motion $\beta_b c$ (i.e., the energy calculated for $p_r=p_\theta=p_z'=0$).

For a thin-beam equilibrium consistent with Eq. (1), the energy variable $\gamma' mc^2$ in Eq. (12) can be approximated by

$$\gamma' mc^2=c(m^2c^2+m^2\hat{\omega}_c^2\rho^2+p_\perp'^2)^{1/2} \tag{13}$$

where use has been made of $P_\theta=P_0$, ρ is defined by

$$\rho=r-R_0 \ , \tag{14}$$

$\hat{\omega}_c=eB_0/mc$ is the nonrelativistic electron cyclotron frequency, and $p_\perp'^2=p_r'^2+p_z'^2$. Substituting Eq. (13) into Eq. (12), and representing

$$\int d^3p'=\int_{-\infty}^{\infty} dp_\theta' \int_0^{2\pi} d\alpha \int_0^{\infty} dp_\perp' p_\perp' \ ,$$

it is straightforward to show that the electron density profile can be expressed as

$$n_e^0(r)=\int d^3p f_e^0(H,P_\theta,P_z)=n_0 \frac{R_0}{r} \Theta(a^2-\rho^2) \ , \tag{15}$$

where

$$a=(\gamma_0^2-1)^{1/2}c/\hat{\omega}_c \tag{16}$$

is the half-thickness of the beam, and $\Theta(x)$ is the Heaviside step function defined by

$$\Theta(x) = \begin{cases} 0 \ , & x<0 \ , \\ 1 \ , & x>0 \ . \end{cases}$$

From Eq. (16), we note that the thin-beam assumption ($a \ll R_0$) is equivalent to the requirement $\gamma_0^2 \ll 1+\hat{\omega}_c^2 R_0^2/c^2$. Since the electron beam is assumed to be thin, we approximate $R_0/r \simeq 1$ in Eq. (15), and the electron density profile reduces to

$$n_e^0(r)=\begin{cases} n_0 , & |r-R_0|<a, \\ 0 , & \text{otherwise} \end{cases} . \tag{17}$$

Making use of $v_z=p_z/\gamma m=(p_z'/m+\gamma'\beta_b c)/(\gamma'+\beta_b p_z'/mc)$, we obtain the axial velocity profile

$$\begin{aligned} V_z^0(r)&=(\int d^3p v_z f_e^0)/(\int d^3p f_e^0) \\ &=\beta_b c=V_b=\text{const.}, \end{aligned} \tag{18}$$

for $|r-R_0|<a$. That is, the axial velocity profile is uniform over the beam cross section. In a similar manner, the azimuthal velocity profile associated with the equilibrium distribution function in Eq. (8) can be expressed as

$$\begin{aligned} V_\theta^0(r)&=(\int d^3p v_\theta f_e^0)/(\int d^3p f_e^0) \\ &= \frac{1}{\gamma_b\gamma_0 m}\left(\frac{P_0}{r}+\frac{e}{2c}\,rB_0\right) . \end{aligned}$$

Making use of $P_0=-e(R_0^2-a^2)B_0/2c$ [definition following Eq. (8)] and the thin-beam assumption ($a<<R_0$), the preceding expression for $V_\theta^0(r)$ can be approximated by

$$V_\theta^0(r) = \frac{eB_0}{\gamma_b\gamma_0 mc}\,\rho = \frac{\omega_c}{\gamma_b}\,\rho \tag{19}$$

for $|r-R_0|<a$.

Finally, for the equilibrium distribution function in Eq. (8), the radial and axial elements of the electron pressure tensor are defined by

$$\begin{aligned} P_{rr}(r)&=T_r^0(r)n_e^0(r)=\int d^3p v_r p_r f_e^0(H,P_\theta,P_z) , \\ P_{zz}(r)&=T_z^0(r)n_e^0(r)=\int d^3p (v_z-V_b)(p_z-\bar{p}_z) f_e^0(H,P_\theta,P_z) , \end{aligned} \tag{20}$$

where $\bar{p}_z=(\int d^3p\ p_z\ f_e^0)/(\int d^3p\ f_e^0)$, $v_r=p_r/\gamma m$, and $T_r^0(r)$ and $T_z^0(r)$ are the

effective radial and axial electron temperature profiles, respectively. Substituting Eq. (12) into Eq. (20), it is straightforward to show that

$$T_r^0(r)=T_z^0(r)=\frac{m\hat{\omega}_c^2}{2\gamma_0\gamma_b}(a^2-\rho^2) \tag{21}$$

for $|r-R_0|<a$. Furthermore, the off-diagonal elements of the equilibrium pressure tensor are identically zero, i.e., $P_{rz}(r)=P_{zr}(r)=0$.

The self-consistent electron density and temperature profiles are illustrated in Fig. 2 for a thin-beam equilibrium. Evidently, for the choice of equilibrium distribution function in Eq. (8), the electron density profile $n_e^0(r)$ is rectangular with sharp radial boundaries [Eq. (17)], the axial velocity profile $V_z^0(r)=\beta_b c$ is uniform over the beam cross section [Eq. (18)], the azimuthal velocity profile $V_\theta^0(r)=\omega_c\rho/\gamma_b$ varies linearly over the beam cross section [Eq. (19)], and the radial and axial temperature profiles are parabolic [Eq. (21)]. Further equilibrium properties of intense hollow beam equilibria described by Eq. (8) are discussed in more detail in Ref. 4 .

III. STABILITY PROPERTIES FOR AZIMUTHALLY SYMMETRIC PERTURBATIONS

A. Linearized Vlasov-Maxwell Equations

In this section, we make use of the linearized Vlasov-Maxwell equations to investigate stability properties for azimuthally symmetric perturbations ($\partial/\partial\theta=0$) about the thin, hollow-beam equilibrium described by Eq. (8). We adopt a normal-mode approach in which all perturbations are assumed to vary with time according to

$$\delta\psi(\underset{\sim}{x},t)=\hat{\psi}(\underset{\sim}{x})\exp\{-i\omega t\} ,$$

with $Im\omega>0$. The Maxwell equations for the perturbed electric and magnetic fields can be expressed as

$$\begin{aligned} \nabla\times\hat{\underset{\sim}{E}}(\underset{\sim}{x}) &= i\,\frac{\omega}{c}\,\hat{\underset{\sim}{B}}(\underset{\sim}{x}) , \\ \nabla\times\hat{\underset{\sim}{B}}(\underset{\sim}{x}) &= \frac{4\pi}{c}\,\hat{\underset{\sim}{J}}(\underset{\sim}{x})-i\,\frac{\omega}{c}\,\hat{\underset{\sim}{E}}(\underset{\sim}{x}) , \end{aligned} \tag{22}$$

where

$$\hat{\underset{\sim}{J}}(\underset{\sim}{x})=-e\int d^3\underset{\sim}{p}\;\underset{\sim}{v}\;\hat{f}_e(\underset{\sim}{x},\underset{\sim}{p}) \tag{23}$$

is the perturbed current density. In Eq. (23),

$$\hat{f}_e(\underset{\sim}{x},\underset{\sim}{p})=e\int_{-\infty}^{0} d\tau\;\exp\{-i\omega\tau\}\left\{\hat{\underset{\sim}{E}}(\underset{\sim}{x}')+\frac{\underset{\sim}{v}'\times\hat{\underset{\sim}{B}}(\underset{\sim}{x}')}{c}\right\}\cdot\frac{\partial}{\partial\underset{\sim}{p}'}\,f_e^0 \tag{24}$$

is the perturbed distribution function, $\tau=t'-t$, and the particle trajectories $\underset{\sim}{x}'(t')$ and $\underset{\sim}{p}'(t')$ satisfy $d\underset{\sim}{x}'/dt'=\underset{\sim}{v}'$ and $d\underset{\sim}{p}'/dt'=-e\underset{\sim}{v}'\times B_0\hat{\underset{\sim}{e}}_z/c$, with "initial" conditions $\underset{\sim}{x}'(t'=t)=\underset{\sim}{x}$ and $\underset{\sim}{p}'(t'=t)=\underset{\sim}{p}$. To make the theoretical analysis tractable, we Fourier decompose the z-dependence of all perturbed quantities according to

$$\hat{\psi}(\underset{\sim}{x})=\int dk\hat{\psi}_k(r)\exp\{ikz\} \tag{25}$$

where k is the axial wavenumber. Note that the perturbation amplitudes in Eq. (25) are independent of θ, because the present stability analysis is restricted to azimuthally symmetric perturbations ($\ell=0$, where ℓ is the azimuthal harmonic number). Making use of Eqs. (22) and (24), it is straightforward to show that

$$\frac{\partial}{\partial r}\hat{B}_{zk}(r)-\frac{cp^2}{r\omega}\hat{\phi}(r)=-\frac{4\pi}{c}\hat{J}_{\theta k}(r) \tag{26}$$

where

$$p^2=\omega^2/c^2-k^2 \tag{27}$$

and the function $\hat{\phi}(r)$ is defined by

$$\hat{\phi}(r)\equiv ir\hat{E}_{\theta k}(r)\ . \tag{28}$$

Equation (26) can be expressed as

$$\frac{\partial}{\partial r}\hat{B}_{zr}(r)=\frac{cp^2}{r\omega}\hat{\phi}(r) \tag{29}$$

in the vacuum region outside the beam, where $\hat{J}_{\theta k}(r)=0$.

The perturbed azimuthal electric field $\hat{E}_{\theta k}(r)$ is continuous across the beam boundaries ($r=R_1$ and $r=R_2$), as is the function $\hat{\phi}(r)$ defined in Eq. (28). For azimuthally symmetric perturbations, it can be shown that (Appendix A)

$$|R_0(\partial\hat{\phi}/\partial r)_{R_0}|\underset{\sim}{<}O[\hat{\phi}(R_0)] \tag{30}$$

where $O[\hat{\phi}(R_0)]$ denotes terms of order $\hat{\phi}(R_0)$. Integrating Eq. (26) from $r=R_1-\delta$ to $r=R_2+\delta$ and taking the limit $\delta\to 0_+$, we obtain the approximate result[17]

$$\hat{B}_{zk}(R_2^+)-\hat{B}_{zk}(R_1^-)=-\frac{4\pi}{c}\int_{R_1^-}^{R_2^+}dr\ \hat{J}_{\theta k}(r) \tag{31}$$

where $\psi(R_j^{\pm})$ denotes $\lim_{\delta\to 0_+} \psi(R_j \pm \delta)$, and use has been made of Eqs. (1) and (30).

Similarly, from Eq. (22), we obtain

$$\frac{\partial}{\partial r}\,[r\hat{B}_{\theta k}(r)]+i\,\frac{r\omega}{c}\,\hat{E}_{zk}(r)=\frac{4\pi}{c}\,r\hat{J}_{zk}(r)\ . \tag{32}$$

Making use of the continuity of $\hat{E}_{zk}(r)$ at $r=R_1$ and $r=R_2$, and the inequality $|R_0(\partial\hat{E}_{zk}/\partial r)_{R_0}|\leq 0[\hat{E}_{zk}(R_0)]$, it is straightforward to show that

$$R_2\hat{B}_{\theta k}(R_2^+)-R_1\hat{B}_{\theta k}(R_1^-)=\frac{4\pi}{c}\int_{R_1^-}^{R_2^+} dr\ r\ \hat{J}_{zk}(r)\ , \tag{33}$$

where again use has been made of $a/R_0<<1$. Substituting

$$\hat{B}_{\theta k}(r)=\frac{i}{cp^2}\,[\omega\,\frac{\partial}{\partial r}\,\hat{E}_{zk}(r)-4\pi k\hat{J}_{rk}(r)] \tag{34}$$

into Eq. (33) gives

$$R_2\left(\frac{\partial\hat{E}_{zk}}{\partial r}\right)_{R_2^+}-R_1\left(\frac{\partial\hat{E}_{zk}}{\partial r}\right)_{R_1^-}=\frac{4\pi}{\omega}\left\{k[R_2\hat{J}_{rk}(R_2^+)-R_1\hat{J}_{rk}(R_1^-)]\right.$$
$$\left.-ip^2\int_{R_1^-}^{R_2^+} dr\ r\ \hat{J}_{zk}(r)\right\}\ . \tag{35}$$

Since the perturbed radial current density vanishes outside the beam, we note that $\hat{J}_{rk}(R_1^-)=\hat{J}_{rk}(R_2^+)=0$. Therefore Eq. (35) can be expressed as

$$R_2\left(\frac{\partial\hat{E}_{zk}}{\partial r}\right)_{R_2^+}-R_1\left(\frac{\partial\hat{E}_{zk}}{\partial r}\right)_{R_1^-}=-i\,\frac{4\pi p^2}{\omega}\int_{R_1^-}^{R_2^+} dr\ r\ \hat{J}_{zk}(r)\ . \tag{36}$$

For convenience, in the subsequent analysis we introduce the normalized electric and magnetic wave admittances,[14-18] $d_{\pm}$ and $b_{\pm}$, defined at the inner and outer surfaces of the electron beam by

$$d_+ = -[r(\partial/\partial r)\hat{E}_{zk}(r)]_{R_2^+}/\hat{E}_{zk}(R_2) \ ,$$
$$d_- = [r(\partial/\partial r)\hat{E}_{zk}(r)]_{R_1^-}/\hat{E}_{zk}(R_1) \ , \tag{37}$$

and

$$b_+ = -\hat{B}_{zk}(R_2^+)/[r(\partial/\partial r)\hat{B}_{zk}(r)]_{R_2} \ ,$$
$$b_- = \hat{B}_{zk}(R_1^-)/[r(\partial/\partial r)\hat{B}_{zk}(r)]_{R_1} \ . \tag{38}$$

For a beam in vacuum, the values of $b_\pm$ and $d_\pm$ depend in detail on the geometric configuration, e.g., location of the conducting wall (Appendix B). It should be noted from Eqs. (22) and (25) that there are two main classes of perturbed fields, i.e., TE and TM perturbations. For the TE mode, the perturbed radial and axial magnetic fields ($\hat{B}_{rk}$ and $\hat{B}_{zk}$) can be expressed as functions of the perturbed azimuthal electric field $\hat{E}_{\theta k}$. On the other hand, for the TM mode, $\hat{E}_{rk}$ and $\hat{B}_{\theta k}$ can be expressed in terms of $\hat{E}_{zk}$. It is therefore convenient to express the right-hand side of Eqs. (31) and (36) as

$$\frac{4\pi\omega}{c^2 p^2}\int_{R_1^-}^{R_2^+} dr\ \hat{J}_{\theta k}(r) = \chi_{11}(\omega)\hat{\phi}(R_0) + iR_0\chi_{12}(\omega)\hat{E}_{zk}(R_0) \ ,$$
$$\frac{4\pi p^2}{\omega}\int_{R_1^-}^{R_2^+} dr\ r\ \hat{J}_{zk}(r) = [\chi_{21}(\omega)/R_0]\hat{\phi}(R_0) - i\chi_{22}(\omega)\hat{E}_{zk}(R_0) \ , \tag{39}$$

where the matrix elements $\chi_{ij}(\omega)$ denote effective susceptibilities.[16,17] Making use of Eqs. (29)-(39), it is straightforward to obtain the approximate results

$$(b_- + b_+)\hat{\phi}(R_0) = \chi_{11}(\omega)\hat{\phi}(R_0) + iR_0\chi_{12}(\omega)\hat{E}_{zk}(R_0) \ ,$$
$$(d_- + d_+)\hat{E}_{zk}(R_0) = i[\chi_{21}(\omega)/R_0]\hat{\phi}(R_0) + \chi_{22}(\omega)\hat{E}_{zk}(R_0) \ . \tag{40}$$

After some simple algebraic manipulation that makes use of Eq. (40), the dispersion relation for azimuthally symmetric perturbations can be expressed as

$$[b_- + b_+ - \chi_{11}(\omega)][d_- + d_+ - \chi_{22}(\omega)] + \chi_{12}(\omega)\chi_{21}(\omega) = 0 \ . \tag{41}$$

Evidently, an explicit evaluation of the susceptibilities $\chi_{ij}(\omega)$ is required for a detailed stability analysis.

B. TE Mode Dispersion Relation

In this section, closed expressions are obtained for the relevant electron susceptibilities [Eq. (39)], and the results are used to derive a simplified TE mode dispersion relation. We specialize to the case of a self-consistent Vlasov equilibrium in which all electrons have the same canonical angular momentum and the same total energy in the moving frame [Eqs. (8) and (12)]. To simplify the right-hand side of Eq. (24), use is made of Eqs. (6) and (9), and the identities $\partial U/\partial \underset{\sim}{p} = \underset{\sim}{v} - V_b \hat{\underset{\sim}{e}}_z$ and $\partial P_\theta / \partial p_\theta = r \hat{\underset{\sim}{e}}_\theta$, where $\hat{\underset{\sim}{e}}_\theta$ is a unit vector in the θ-direction. The perturbed distribution function can then be expressed as

$$\hat{f}_{ek}(r, \underset{\sim}{p}) = \hat{f}^E_{ek}(r, \underset{\sim}{p}) + \hat{f}^M_{ek}(r, \underset{\sim}{p}) \ ,$$

where

$$\hat{f}^E_{ek}(r, \underset{\sim}{p}) = e \int_{-\infty}^{0} d\tau \exp\{i[k(z'-z) - \omega\tau]\} \left\{ \left(1 - \frac{kV_b}{\omega}\right) \hat{E}_{\theta k}(r') \, v'_\theta \, \frac{\partial f_e^0}{\partial U} \right.$$
$$\left. + r' \left[\left(1 - \frac{kv'_z}{\omega}\right) \hat{E}_{\theta k}(r') - \frac{v'_r}{c} \hat{B}_{zk}(r') \right] \frac{\partial f_e^0}{\partial P_\theta} \right\} \tag{42}$$

is that portion of the perturbed distribution function that is generated from the TE perturbation, and

$$\hat{f}^{M}_{ek}(r,p)=e\frac{\partial f^{0}_{e}}{\partial U}\int_{-\infty}^{0} d\tau\ \exp\{i[k(z'-z)-\omega\tau]\}\{[\hat{E}_{rk}(r')-\beta_b\hat{B}_{\theta k}(r')]v'_r + \hat{E}_{zk}(r')(v'_z-V_b)\} \tag{43}$$

is that portion of $\hat{f}_{ek}$ that is generated from the TM perturbation.

As indicated in Eqs. (42) and (43), the particle trajectories, $r'(\tau)$, $\theta'(\tau)$, $z'(\tau)$, in the equilibrium field configuration are required in order to evaluate the perturbed distribution function. Making use of Eqs. (5) and (6), and $P_\theta=P_0=-(e/2c)(R_0^2-a^2)B_0$ [see discussion following Eq. (8)], it is straightforward to obtain the required trajectories. Assuming that the electron orbit passes through the phase-space point (ρ,p_r) and (z,p_z) at time $t'=t$, we find

$$\begin{aligned}
\rho' &= \rho\cos(\hat{\omega}_c/\gamma)\tau+(p_r/m\hat{\omega}_c)\sin(\hat{\omega}_c/\gamma)\tau\ , \\
z' &= z+(p_z/\gamma m)\tau\ , \\
\dot{\theta}' &= (\hat{\omega}_c/\gamma R_0)[\rho\cos(\hat{\omega}_c/\gamma)\tau+(p_r/m\hat{\omega}_c)\sin(\hat{\omega}_c/\gamma)\tau]\ ,
\end{aligned} \tag{44}$$

where $\rho=r-R_0$, $\hat{\omega}_c=eB_0/mc$ is the nonrelativistic electron cyclotron frequency and use has been made of Eq. (1).

From Eqs. (39) and (42), the matrix element $\chi_{11}(\omega)$ is determined from

$$\chi_{11}(\omega)\hat{\phi}(R_0)=\frac{4\pi\omega}{c^2p^2}\int_{R_1^-}^{R_2^+} dr\ \hat{J}^{E}_{\theta k}(r)\ , \tag{45}$$

where the perturbed azimuthal current density corresponding to the TE mode is defined by

$$\hat{J}^{E}_{\theta k}(r)=-e\int d^3p\ v_\theta\ \hat{f}^{E}_{ek}(r,p)\ . \tag{46}$$

For present purposes it is also assumed that

$$|\omega-kV_b-\omega_c/\gamma_b|<<\omega_c/\gamma_b \tag{47}$$

where $\omega_c=eB_0/\gamma_0 mc$ is the electron cyclotron frequency in a frame of reference moving with axial velocity V_b. Within the context of Eqs. (1), (30), and (47) it is valid to approximate

$$\hat{\phi}(r')=ir'\hat{E}_{\theta k}(r')\simeq\hat{\phi}(R_0) \tag{48}$$

and to neglect the terms proportional to $\partial f_e^0/\partial P_\theta$ in Eq. (42), since the corrections associated with these terms are of order $\gamma_b|\omega-kV_b-\omega_c/\gamma_b|/\omega_c$, a/R_0 (<<1), or smaller. Substituting Eq. (48) into Eq. (42), the perturbed distribution function in Eq. (42) can then be approximated by

$$\hat{f}_{ek}^E(r,\underset{\sim}{p})=-ie\left(1-\frac{kV_b}{\omega}\right)\frac{\partial f_e^0}{\partial U}\int_{-\infty}^{0}d\tau\,\dot{\theta}'\exp\{i[k(z'-z)-\omega\tau]\} \tag{49}$$

where use has been made of $v_\theta'=r'\dot{\theta}'$. Since the variable U is an even function of p_r [Eq. (9)], we note from Eqs. (46) and (49) that any portion of the time integral in Eq. (49) that is an odd function of p_r will automatically give zero when the integration over p_r is carried out. Therefore, we simply omit terms proportional to odd functions of p_r when calculating $\hat{f}_{ek}^E$ from Eq. (49). Making use of Eqs. (44) and (47), the perturbed distribution function for the TE mode is given by

$$\hat{f}_{ek}^E(r,\underset{\sim}{p})=\frac{e\rho}{2R_0}\left(1-\frac{kV_b}{\omega}\right)\frac{\partial f_e^0}{\partial U}\frac{\hat{\omega}_c\hat{\phi}(R_0)}{\gamma\omega-\hat{\omega}_c-kp_z/m}\,, \tag{50}$$

where $\hat{\omega}_c=eB_0/mc$.

The integral $\int d^3p\, v_\theta\, \hat{f}_{ek}^E$ is required to evaluate the perturbed azimuthal current density. For a thin, hollow beam, we note from Eq. (44) that $v_\theta=r\dot{\theta}$ can be approximated by

$$v_\theta=\rho\hat{\omega}_c/\gamma\quad. \tag{51}$$

Substituting Eqs. (8), (50), and (51) into Eq. (46), making use of the transformations in Eq. (10), and carrying out the required integration over momentum, the perturbed azimuthal current density corresponding to the TE mode can be expressed as

$$\hat{J}^{E}_{\theta k}(r) = \frac{e^2 n_0 \rho^2}{2\gamma_b \gamma_0 m R_0}\left(1-\frac{kV_b}{\omega}\right)\hat{\phi}(R_0)\left\{\frac{\delta(\rho-a)+\delta(\rho+a)}{a(\omega-kV_b-\omega_c/\gamma_b)}\right.$$
$$\left.-\frac{\omega_c^2 c[(\omega-kV_b)(\omega-kV_b-\omega_c/\gamma_b)-(\omega\beta_b-kc)^2]\Theta(a^2-\rho^2)}{[c^2(\omega-kv_b-\omega_c/\gamma_b)^2-(\omega\beta_b-kc)^2\omega_c^2(a^2-\rho^2)]^{3/2}}\right\}, \tag{52}$$

where $\omega_c=eB_0/\gamma_0 mc$ is the electron cyclotron frequency in the moving frame. Substituting Eq. (52) into Eq. (45), we find

$$\chi_{11}(\omega) = \frac{\omega_p^2}{\gamma_b}\frac{(\omega-kV_b)^2}{c^2 p^2 (kc-\omega\beta_b)^2 R_0}\left\{a-\frac{c[\Omega-(kc-\omega\beta_b)^2/(\omega-kV_b)]}{2\omega_c(kc-\omega\beta_b)}\right.$$
$$\left.\times \ell n\left[\frac{c\Omega+\omega_c a(kc-\omega\beta_b)}{c\Omega-\omega_c a(kc-\omega\beta_b)}\right]\right\}, \tag{53}$$

where $\omega_p^2=4\pi n_0 e^2/\gamma_0 m$ is the electron plasma frequency squared in the moving frame, and Ω is the Doppler shifted frequency defined by

$$\Omega=\omega-kV_b-\omega_c/\gamma_b \ . \tag{54}$$

The following point of verification is noteworthy. If instead we make use of the equilibrium distribution function (characterized by $V_z^0=0$)

$$f_e^0(H,P_\theta) = \frac{n_0 R_0}{2\pi\gamma_0 m}\delta(H-\gamma_0 mc^2)\delta(P_\theta-P_0) \ ,$$

and then make the appropriate relativistic transformation to a frame of reference moving with axial velocity $-\beta_b c\hat{e}_z$, then the expression obtained for $\chi_{11}(\omega)$ is identical to Eq. (53).

Following similar algebraic manipulations, we have evaluated the remaining susceptibility matrix elements χ_{12}, χ_{21}, and χ_{22}.

However, after some straightforward but tedious algebra, it is found that

$$\left|\frac{\chi_{21}}{\chi_{11}}\right| , \quad \left|\frac{\chi_{22}}{\chi_{11}}\right| \lesssim \left|\frac{\Omega}{\omega_{ce}}\right| , \quad \frac{a}{R_0} << 1 . \tag{55}$$

Therefore, within the context of the inequalities in Eq. (55), the TE mode dispersion relation obtained from Eq. (41) can be approximated by

$$b_- + b_+ = \chi_{11}(\omega) . \tag{56}$$

In Sec. IV, we make use of the approximate dispersion relation in Eq. (56) to investigate TE mode stability properties for azimuthally symmetric perturbations about the hollow-beam equilibrium described by Eq. (8).

IV. TE MODE STABILITY ANALYSIS FOR AZIMUTHALLY SYMMETRIC PERTURBATIONS

Within the context of Eq. (55), the TE mode is the dominant unstable perturbation. In this section, we make use of Eqs. (53) and (56) to investigate TE mode stability properties in parameter regimes of experimental interest.[21-24]

The number of electrons per unit axial length can be expressed as $N_e=4\pi n_0 a R_0$. Eliminating n_0 in favor of N_e in Eq. (53) and substituting Eq. (53) into Eq. (56), the TE mode dispersion relation is given by

$$b_-+b_+ = \frac{\nu}{\gamma_b\gamma_0}\frac{(\omega-kV_b)^2}{p^2R_0^2(kc-\omega\beta_b)^2}\left\{1-\frac{[\Omega-(kc-\omega\beta_b)^2/(\omega-kV_b)]}{2\beta_0(kc-\omega\beta_b)}\right. \times \left.\ell n\left(\frac{\Omega+\beta_0(kc-\omega\beta_b)}{\Omega-\beta_0(kc-\omega\beta_b)}\right)\right\}, \tag{57}$$

where $\nu\equiv N_e e^2/mc^2$ is Budker's parameter, $\beta_0\equiv(1-1/\gamma_0^2)^{1/2}$, and use has been made of Eq. (16). The growth rate $\omega_i=\mathrm{Im}\omega$ and real oscillation frequency $\omega_r=\mathrm{Re}\omega$ can be determined from Eq. (57) for a broad range of system parameter, by solving numerically the full transcendental dispersion relation. We reiterate that Eq. (57) is valid only when $|\Omega|=|\omega-kV_b-\omega_c/\gamma_b|<<\omega_c/\gamma_b$ [Eq. (47)]. Moreover, it should be noted that the magnetic wave admittances $b_\pm$ defined in Eq. (B.3) are generally complicated functions of the eigenfrequency $\omega=\omega_r+i\omega_i$.

A. Limit of a Tenuous, Infinitesimally Thin Beam

To simplify the expressions for the magnetic wave admittances $b_\pm$ defined in Eq. (B.3), it is useful to consider the limit where the electron beam is infinitesimally thin,

$$a/R_0 \to 0 \ , \tag{58}$$

and the beam density is very tenuous, i.e.,

$$\nu/\gamma_0 \to 0 \ . \tag{59}$$

Making use of Eq. (58), it is straightforward to show from Eq. (B.3) in Appendix B that b_-+b_+ can be approximated by

$$b_-+b_+ = -\frac{2J_1(pR_c)/\pi p^2 R_0^2}{J_1(pR_0)[J_1(pR_0)N_1(pR_c)-J_1(pR_c)N_1(pR_0)]} \ , \tag{60}$$

where $p^2=\omega^2/c^2-k^2$, $J_1(x)$ and $N_1(x)$ are Bessel functions of first and second kind, respectively, and use has been made of $N_0(x)J_1(x)-J_0(x)N_1(x)=2/\pi x$. In the absence of a beam, the vacuum TE mode dispersion relation is given by

$$p^2R_c^2=(\omega^2/c^2-k^2)R_c^2=\alpha_{0n}^2 \ , \tag{61}$$

where α_{0n} is the nth root of $J_1(\alpha_{0n})=0$. For a very tenuous beam [Eq. (59)], it is evident from Eqs. (57) and (60) that Eq. (61) is a good approximation to the dispersion relation in Eq. (57). [The right-hand side of Eq. (57) describes the beam-produced modifications to the vacuum dispersion relation (61).] Taylor expanding Eq. (60) about $(\omega^2/c^2-k^2)R_c^2=\alpha_{0n}^2$, it is straightforward to show that b_-+b_+ can be approximated in leading order by

$$b_-+b_+ = \frac{1}{2p^2}\left(\frac{R_c}{R_0}\right)^2\left(\frac{\omega^2}{c^2}-k^2-\frac{\alpha_{0n}^2}{R_c^2}\right)\left[\frac{J_2(\alpha_{0n})}{J_1(\alpha_{0n}R_0/R_c)}\right]^2 \ . \tag{62}$$

Substituting Eq. (62) into Eq. (57), we obtain the approximate dispersion relation

$$\frac{\omega^2}{c^2} - k^2 - \frac{\alpha_{0n}^2}{R_c^2} = \frac{2\nu}{\gamma_b\gamma_0}\left[\frac{J_1(\alpha_{0n}R_0/R_c)}{R_c J_2(\alpha_{0n})}\right]^2\left(\frac{\omega-kV_b}{kc-\omega\beta_b}\right)^2 \times\left\{1-\frac{\Omega-(kc-\omega\beta_b)^2/(\omega-kV_b)}{2\beta_0(kc-\omega\beta_b)}\,\ell n\left[\frac{\Omega+\beta_0(kc-\omega\beta_b)}{\Omega-\beta_0(kc-\omega\beta_b)}\right]\right\} \tag{63}$$

for a tenuous, infinitesimally thin beam.

To lowest order, the eigenfrequency ω and axial wavenumber k are obtained from the simultaneous solution of Eq. (61) (the vacuum TE mode dispersion relation) and the condition for cyclotron resonance [Eq. (47)]

$$\omega \simeq kV_b + \omega_c/\gamma_b \ . \tag{64}$$

In addition, as shown in Appendix C, the region of k space <u>corresponding to instability</u> is very narrow-band with

$$kc \simeq \omega\beta_b \ . \tag{65}$$

Solving Eqs. (64) and (65) for the characteristic frequency and wavenumber $(\omega,k)\equiv(\omega_0,k_0)$, we find (Fig. 3)

$$\omega_0 = \omega_c\gamma_b \ , \qquad k_0 = \omega_c\gamma_b\beta_b/c \ , \tag{66}$$

where use has been made of $\gamma_b=(1-\beta_b^2)^{-1/2}$. Since, for a very tenuous beam, we also require that (ω_0,k_0) solve Eq. (61) in leading order, it follows that instability exists only in the narrow region of parameter space satisfying

$$\frac{\omega_c}{c} \simeq \frac{\alpha_{0n}}{R_c} \quad . \tag{67}$$

This feature is also evident from the numerical studies of the dispersion relation presented in Sec. IV.B. Finally, for future reference, it should be noted from Eqs. (61) and (65) that the group velocity can be approximated by

$$V_g = \frac{d\omega}{dk} = \frac{kc^2}{\omega} \simeq V_b \quad . \tag{68}$$

That is, for a very tenuous beam, the group velocity of the unstable waves is approximately equal to the beam velocity.

Appendix C and the previous paragraph give some useful insight into the region of parameter space corresponding to instability. Most important is the fact that the instability is narrow-band in k-space with $|kc-\omega\beta_b| \ll c/R_0$ [Appendix C and Eq. (65)]. Expanding the logarithmic contribution for small $|kc-\omega\beta_b|$, the dispersion relation in Eq. (63) can be expressed in the approximate form

$$\frac{\omega^2}{c^2} - k^2 - \frac{\alpha_{0n}^2}{R_c^2} = \frac{2\nu}{\gamma_b\gamma_0}\left(\frac{J_1(\alpha_{0n}R_0/R_c)}{R_c J_2(\alpha_{0n})}\right)^2 \left[\frac{\omega-kV_b}{\omega-kV_b-\omega_c/\gamma_b} - \frac{\beta_0^2(\omega-kV_b)^2}{3(\omega-kV_b-\omega_c/\gamma_b)^2}\right] , \tag{69}$$

where $\beta_0=(1-1/\gamma_0^2)^{1/2}$. The general features of Eq. (69) are qualitatively similar to the result obtained by Friedman et al.[21] for perturbations about a self-consistent Vlasov equilibrium, $f_e^0=\text{const.}\times\delta(H_\perp-\gamma_0 mc^2) \times \delta(p_z-\gamma_b m\beta_b c)\delta(P_\theta-P_0)$, where all electrons have the same perpendicular energy $H_\perp=\gamma_0 mc^2$. As indicated in the introduction, however, Eq. (69) differs in detail as do the corresponding stability results. For example, the last term on the right-hand side of Eq. (69) is proportional to $\beta_0^2(\omega-kV_b)^2/3$, instead of $\beta_0^2(\omega^2-k^2c^2)/2$ as obtained in

Ref. 21. Therefore, depending on the region of parameter space, the stability properties obtained from Eq. (69) can differ considerably from the results obtained in previous analyses of the cyclotron maser instability.[21] Moreover, the dispersion relation in Eq. (63) predicts instability for a very narrow range of k-values, whereas previous studies[21] have not been able to identify the range of unstable k values in a consistent manner.

Finally, the necessary and sufficient condition for Eq. (69) to have unstable solutions ($\mathrm{Im}\omega>0$) is given by

$$\beta_0^4 > \frac{4}{3}\frac{\nu c^2}{\gamma_0\gamma_b\omega_c^2}\left[\frac{J_1(\alpha_{0n}R_0/R_c)}{R_c J_2(\alpha_{0n})}\right]^2 , \tag{70}$$

which is qualitatively similar to the result obtained by Sprangle and Drobot[10] for a non-self-consistent equilibrium slab configuration.

B. Numerical Analysis of Dispersion Relation

In this section we make use of the dispersion relation (57) to carry out a numerical investigation of stability properties. In this regard, no a priori assumption is made that the beam is very tenuous (as in Sec. IV.A). However, use is made of the fact that the narrow-band of unstable k values satisfies $|kc-\omega\beta_b|<<c/R_0$. Expanding the logarithm in Eq. (57), and evaluating k, p^2, and $b_+ + b_-$ at $(\omega,k)=(\omega_0,k_0)$ [Eq. (66)], the dispersion relation (57) can be approximated by

$$\hat{p}^2(\hat{b}_-+\hat{b}_+)+(\omega-\omega_0)\left[\frac{d}{d\omega}(b_-+b_+)\right]_{\omega_0,k_0} = \frac{\nu}{\gamma_b\gamma_0 R_0^2}\frac{(\omega-k_0V_b)}{(\omega-k_0V_b-\omega_c/\gamma_b)} \times\left[1-\frac{\beta_0^2}{3}\frac{(\omega-k_0V_b)}{(\omega-k_0V_b-\omega_c/\gamma_b)}\right] , \tag{71}$$

where $\hat{p}^2\equiv\omega_0^2/c^2-k_0^2$, and $\hat{b}_-+\hat{b}_+\equiv[b_-+b_+]_{\omega_0,k_0}$ is defined by Eq. (B.3).

The growth rate $\omega_i=\text{Im}\omega$ and real oscillation frequency $\omega_r=\text{Re}\omega$ have been calculated numerically from Eq. (71) for a broad range of system parameters a/R_0, R_c/R_0, ν, β_b and β_0. For R_c/R_0 corresponding to $\hat{b}_-+\hat{b}_+\simeq 0$, we have Taylor expanded (b_-+b_+) about $\omega=\omega_0$, approximating (b_-+b_+) in leading order by $(b_-+b_+)=(\omega-\omega_0)[d(b_-+b_+)/d\omega]_{\omega_0,k_0}$. For present purposes, to illustrate the influence of the geometric configuration on stability behavior, we calculate the normalized magnetic wave admittances $\hat{b}_\pm$. Shown in Fig. 4(a) is a plot of $\hat{b}_+\hat{b}_-$ versus R_c/R_0, for $\beta_0=0.2$, $\beta_b=0.143$ and $a/R_0=0.1$. It is evident from Fig. 4(a) that $\hat{b}_-+\hat{b}_+=0$ for $R_c/R_0=2.18$ and $R_c/R_0=3.75$, which corresponds to the TE mode dispersion relation without beam-produced modifications. Figure 4(b) shows a plot of the normalized growth rate ω_i/ω_c versus R_c/R_0 obtained from Eq. (71) for $\nu=0.001$ and parameters otherwise identical to Fig. 4(a). Two important features are noteworthy from Fig. 4. First, for a low beam density ($\nu\lesssim 0.001$), the <u>maximum</u> growth rate occurs at the value of R_c/R_0 for which $\hat{b}_-+\hat{b}_+$ is equal to zero. For example, in Fig. 4(b), the system is most unstable at $R_c/R_0=2.18$. Second, for a low beam density, the system is unstable only in the range where $\hat{b}_-+\hat{b}_+\gtrsim 0$ [compare Figs. 4(a) and 4(b)].

Shown in Fig. 5(a) is a plot of $(\hat{b}_-+\hat{b}_+)$ versus R_c/R_0 for $\beta_0=0.4$, $\beta_b=0.286$ and $a/R_0=0.2$. Also shown in Fig. 5(b) are plots of the normalized Doppler shifted real frequency $\text{Re}(\Omega/\omega_c)=(\omega_r-kV_b-\omega_c/\gamma_b)/\omega_c$ and growth rate ω_i/ω_c versus R_c/R_0 for $\nu=0.001$ and parameters otherwise identical to Fig. 5(a). Note that $\text{Re}(\Omega/\omega_c)$ is plotted only for the range of R_c/R_0 corresponding to instability. Evidently, for the low beam density in Fig. 5, the stability properties are qualitatively similar to those in Fig. 4. However, it is also evident from Figs. 4(b) and 5(b) that the growth rate increases rapidly as β_0 is

increased. Moreover, we note from Fig. 5(b) that $Re\Omega/\omega_c$ assumes a maximum value (0.019) at $R_c/R_0=2.375$ and decreases rapidly to zero when R_c/R_0 is increased.

We conclude this section by emphasizing that stability properties also exhibit a sensitive dependence on beam density. This is illustrated in Fig. 6 where the normalized growth rate ω_i/ω_c is plotted versus R_c/R_0 for two different values of ν, and parameters otherwise identical to Fig. 5(a). For intermediate or high beam densities ($\nu \gtrsim 0.01$), the maximum growth rate no longer coincides with values of R_c/R_0 for which $(\hat{b}_-+\hat{b}_+)=0$. For example, in Fig. 6, the maximum growth rate occurs for $R_c/R_0=2.45$ when $\nu=0.01$, and for $R_c/R_c=2.51$ when $\nu=0.1$. Evidently, the value of R_c/R_0 corresponding to maximum growth rate is a slowly increasing function of beam density. However, the value of the maximum growth rate increases relatively rapidly with increasing beam density. We also note, for high beam densities, that the system can be unstable even for negative values of $(\hat{b}_-+\hat{b}_+)$ (Fig. 6). This is not the case for low beam densities (Fig. 4).

V. CONCLUSIONS

In this paper we have formulated a self-consistent theory of the cyclotron maser instability. The stability analysis was carried out for an infinitely long hollow beam propagating parallel to a uniform magnetic field $B_0\hat{e}_z$, within the framework of the linearized Vlasov-Maxwell equations. The equilibrium configuration and basic assumptions were summarized in Sec. II.A. In Sec. II.B, equilibrium properties were calculated for the choice of electron distribution function in which all electrons have the same value of canonical angular momentum (P_0) and the same value of energy ($\gamma_0 mc^2$) in a frame of reference moving with axial velocity $\beta_b c$ [Eq. (8)]. Stability properties for azimuthally symmetric perturbations were examined in Secs. III and IV. As shown in Sec. III.B, the TE mode corresponds to the most unstable perturbation. Moreover, the analysis in Appendix C predicted that instability occurs for a very narrow range of k values satisfying $|kc-\beta_b\omega| \ll c/R_0$. A detailed numerical analysis of the approximate dispersion relation (71) was presented in Sec. IV.B. One of the most important conclusions of this study is that the geometric configuration $(\hat{b}_-+\hat{b}_+)$ has a large influence on stability behavior, particularly when the beam density is low. Moreover, the maximum growth rate increases relatively rapidly with increasing beam density.

ACKNOWLEDGMENTS

This research was supported by the National Science Foundation, the Office of Naval Research under the auspices of the University of Maryland-Naval Research Laboratory Joint Program in Plasma Physics, the Naval Electronic Systems Command, Task PDM3012, and the Army Ballistic Missile Defence Advanced Technology Center, MIPR W31RPD-83 Z 107.

APPENDIX A

EVALUATION OF PERTURBED AZIMUTHAL ELECTRIC FIELD

From Eqs. (22) and (28), we find that

$$\frac{d}{dr}\hat{\phi}(r) = -\frac{r\omega}{c}\hat{B}_{zk}(r) \ . \tag{A.1}$$

Since the perturbed azimuthal current density is even function of ρ [Eq. (52)], it is straightforward to show that

$$\hat{B}_{zk}(R_0) = \frac{1}{2}\left[\hat{B}_{zk}(R_2^+)+\hat{B}_{zk}(R_1^-)\right] \ . \tag{A.2}$$

Making use of Eqs. (29), (38), (A.1) and (A.2), we obtain

$$R_0(d\hat{\phi}/dr)_{R_0}/\hat{\phi}(R_0) \simeq \frac{1}{2}p^2R_0^2(b_+-b_-) \ . \tag{A.3}$$

From Eq. (A.3), it follows that

$$|R_0(d\hat{\phi}/dr)_{R_0}| \lesssim 0[\hat{\phi}(R_0)] \ , \tag{A.4}$$

provided $|p^2R_0^2(b_+-b_-)| \lesssim 1$.

APPENDIX B

EVALUATION OF MAGNETIC WAVE ADMITTANCES

In this section, we obtain expressions for the wave admittances at the boundaries of a hollow electron beam in a cylindrical waveguide. Since the perturbed current density vanishes in the vacuum region outisde the beam, Maxwell's equation in this region can be expressed as

$$(\frac{1}{r}\frac{\partial}{\partial r} r \frac{\partial}{\partial r} + p^2)\hat{B}_{zk}(r)=0 \tag{B.1}$$

where $p^2=\omega^2/c^2-k^2$. In obtaining Eq. (B.1), use has been made of Eqs. (29) and (A.1). The solution to Eq. (B.1) is given by

$$\hat{B}_{zk}(r) = \begin{cases} AJ_0(pr)+BN_0(pr) , & R_2<r<R_c , \\ CJ_0(pr) , & 0<r<R_1 , \end{cases} \tag{B.2}$$

where $J_0(pr)$ and $N_0(pr)$ are Bessel functions of the first and second kind, respectively, and R_c is the radius of the waveguide (Fig. 1). In Eq. (B.2), the constants A, B, and C are related by Eq. (28) and the boundary condition $[(\partial/\partial r)\hat{B}_{zk}(r)]_{R_c}=0$. After some straightforward algebra, the magnetic wave admittances defined in Eq. (38) can be expressed as

$$b_+ = \frac{1}{R_2 p}\frac{J_0(pR_2)N_1(pR_c)-J_1(pR_c)N_0(pR_2)}{J_1(pR_2)N_1(pR_c)-J_1(pR_c)N_1(pR_2)} ,$$

$$b_- = -\frac{1}{R_1 p}\frac{J_0(pR_1)}{J_1(pR_1)} , \tag{B.3}$$

where R_1 and R_2 are the inner and outer radii of the beam, and use has been made of $dJ_0(x)/dx=-J_1(x)$ and $dN_0(x)/dx=-N_1(x)$. Closed expressions for the electric wave admittances $d_\pm$ [Eq. (37)] can be obtained in a similar manner[17] but are not required in the TE mode stability analysis in Sec. IV.

APPENDIX C

NYQUIST STABILITY ANALYSIS FOR PERTURBATIONS WITH $k \neq \beta_b \omega/c$

In this section, we make use of the Nyquist method to obtain necessary and sufficient conditions for instability from the TE mode dispersion relation [Eq. (57)].[15,26] The analysis is carried out for perturbations with the axial wavenumber k satisfying

$$q = k - \beta_b \omega/c \neq 0 \ . \tag{C.1}$$

Consistent with Eq. (47), for present purposes we approximate $\omega \simeq kV_b + \omega_c/\gamma_b$ in the definitions of q [Eq. (C.1)], $p^2 = \omega^2/c^2 - k^2$, and the magnetic wave admittances $b_\pm$ [Eq. (B.3)]. Assuming $(b_- + b_+) \neq 0$, and defining

$$\begin{aligned} z &= \Omega/\beta_0 qc = (\omega - kV_b + \omega_c/\gamma_b)/\beta_0 qc \ , \\ s &= qc\gamma_b/\beta_0\omega_c \ , \\ \alpha &= c^2 p^2 R_0^2 \gamma_0 \gamma_b^3/\nu\omega_c^2 \ , \end{aligned} \tag{C.2}$$

it is straightforward to express the TE mode dispersion relation in Eq. (57) as

$$D(z) = (z-s)\,\ell n\left(\frac{z+1}{z-1}\right) - 2 = -2(b_- + b_+)q^2\alpha \ , \tag{C.3}$$

where the complex variable z is defined in Eq. (C.2). Note from Eq. (C.3) that the dispersion relation is an even function of q so that stability properties do not depend on the sign of q. Therefore, we assume $q > 0$ without loss of generality.

Nyquist plots of the function D(z) defined in Eq. (C.3), which map the upper half z plane (contour Γ) onto the complex D plane

(contour Γ'), enable us to study the stability properties predicted by Eq. (C.3) [Figs. 7 and 8]. Figures 7(a) and 8(a) are plots of contour Γ for $s<1$ and $s>1$, respectively. Branch cuts originating from the branch points at $z=\pm 1$ must be introduced, as shown in Figs. 7(a) and 8(a), to make the function $D(z)$ single valued. Plots of $D(z)$ are shown in Fig. 7(b) for $s<1$, and in Fig. 8(b) for $s>1$. In obtaining the contour Γ' in Figs. 7(b) and 8(b), use has been made of the definition $\ell nz=\ell nr+i\theta$ $(-\pi<\theta\leq\pi)$, where $z=r\exp\{i\theta\}$.

The Nyquist analysis indicates that the system is stable ($Im\Omega\leq 0$) provided the contour Γ' in the complex D plane does not enclose the point $-2(b_-+b_+)q^2\alpha$. Therefore, it follows from Figs. 7(b) and 8(b) that a necessary condition for instability is

$$s<1 \ . \tag{C.4}$$

Moreover, from Fig. 7(b), we also note that

$$0<(b_-+b_+)q^2\alpha<1 \tag{C.5}$$

is a necessary condition for instability. Since $q^2\alpha>0$, we conclude that $(b_-+b_+)>0$ is required for instability, which is consistent with the results obtained from a numerical analysis of the dispersion relation (see Fig. 4). Combining the two inequalities in Eqs. (C.4) and (C.5), and making use of Eq. (C.2), it is straightforward to show for typical beam parameters that

$$|q|=|k-\beta_b\omega/c|<<1/R_0 \tag{C.6}$$

is required for instability, which corresponds to a very <u>narrow</u> bandwidth in k-space. The inequality in Eq. (C.6) can also be demonstrated for the case $(b_-+b_+)\simeq 0$, by Taylor-expanding (b_-+b_+)

about $\omega=kV_b+\omega_c/\gamma_b$, keeping first-order terms in Ω, and making use of $[d(b_-+b_+)/d\omega]_{kV_b+\omega_c/\gamma_b}>0$.

REFERENCES

1. K. D. Marx, Phys. Fluids 11, 357 (1968).
2. R. C. Davidson, A. T. Drobot, and C. A. Kapetanakos, Phys. Fluids 16, 2199 (1973).
3. R. C. Davidson and S. M. Mahajan, Phys. Fluids 17, 2090 (1974).
4. R. C. Davidson and C. D. Striffler, J. Plasma Physics 12, 353 (1974).
5. R. H. Levy, Phys. Fluids 8, 1288 (1965).
6. R. C. Davidson, H. Uhm, and S. M. Mahajan, Phys. Fluids 19, 1608 (1976).
7. R. V. Lovelace, Phys. Rev. Lett. 35, 162 (1975).
8. E. Ott and W. M. Manheimer, IEEE Trans. PS-3, 1 (1975).
9. P. Sprangle and W. M. Manheimer, Phys. Fluids 18, 224 (1975).
10. P. Sprangle and A. T. Drobot, IEEE Trans. MTT-25, 528 (1977).
11. K. R. Chu and J. L. Hirshfield, Phys. Fluids, in press (1977).
12. P. Sprangle, J. Appl. Phys. 49, 2935 (1976).
13. H. Uhm and R. C. Davidson, J. Appl. Phys., in press (1977).
14. R. J. Briggs and V. K. Neil, Plasma Phys. 9, 209 (1967).
15. Y. Y. Lau and R. J. Briggs, Phys. Fluids 14, 967 (1971).
16. H. Uhm and R. C. Davidson, Phys. Fluids 20, 771 (1977).
17. H. Uhm and R. C. Davidson, Phys. Fluids 21, in press (1978).
18. Y. Goren, H. Uhm, and R. C. Davidson, J. Appl. Phys., in press (1978).
19. C. A. Kapetanakos, D. A. Hammer, C. D. Striffler, and R. C. Davidson, Phys. Rev. Lett. 30, 1303 (1973).
20. H. A. Davis, R. A. Meger and H. H. Fleischmann, Phys. Rev. Lett. 37, 542 (1976).
21. M. Friedman, D. A. Hammer, W. M. Manheimer, and P. Sprangle, Phys. Rev. Lett. 31, 753 (1973).
22. V. L. Granatstein, P. Sprangle, R. K. Parker, J. Pasour, M. Herndon, and S. P. Schlesinger, Phys. Rev. A14, 1194 (1976).

23. N. I. Zaytsev, T. B. Pankratova, M. I. Petelin, and V. A. Flyagin, Radio Engineering and Electronic Physics 19, 103 (1974).

24. D. V. Kisel , G. S. Korablev, V. G. Navelyev, M. I. Petelin, and Sh. E. Tsimring, Radio Engineering and Electronic Physics 19, 95 (1974).

25. W. W. Destler, D. W. Hudgings, M. J. Rhee, S. Kawasaki, and V. L. Granatstein, J. Appl. Phys. 48, 3291 (1977).

26. N. A. Krall and A. W. Trivelpiece, Principles of Plasma Physics (McGraw Hill Book Company, New York, 1973), Ch. 9.

FIGURE CAPTIONS

Fig. 1 Equilibrium configuration and coordinate system.

Fig. 2 Electron density [Eq. (17)] and temperature profiles [Eq. (21)].

Fig. 3 The straight lines $\omega=kV_b+\omega_c/\gamma_b$ and $\omega=kc/\beta_b$ intersect at $(\omega_0,k_0)=(\omega_c\gamma_b,\ \beta_b\omega_c\gamma_b/c)$. The curve $\omega=(c^2k^2+\alpha_{0n}^2c^2/R_c^2)^{1/2}$ passes through (ω_0,k_0) provided $\alpha_{0n}c/R_c=\omega_c$.

Fig. 4 (a) Plot of sum of magnetic wave admittances (b_-+b_+) (Appendix B) versus R_c/R_0, for $\beta_0=0.2$, $\beta_b=0.143$ and $a/R_0=0.1$. (b) Plot of normalized growth rate ω_i/ω_c versus R_c/R_0 [Eq. (68)], for $\nu=0.001$ and parameters otherwise identical to Fig. 4(a).

Fig. 5 (a) Plot of sum of magnetic wave admittances (b_-+b_+) (Appendix B) versus R_c/R_0, for $\beta_0=0.4$, $\beta_b=0.286$ and $a/R_0=0.2$. (b) Plot of the normalized Doppler shifted real frequency $Re\Omega/\omega_c=Re(\omega-kV_b-\omega_c/\gamma_b)/\omega_c$ and growth rate ω_i/ω_c versus R_c/R_0 [Eq. (68)], for $\nu=0.001$ and parameters otherwise identical to Fig. 5(a).

Fig. 6 Plot of normalized growth rate ω_i/ω_c versus R_c/R_0 [Eq. (68)], for $\nu=0.01$ and $\nu=0.1$, and parameters otherwise identical to Fig. 5(a).

Fig. 7 Map of upper-half z plane (contour Γ) onto the D plane (contour Γ') for $s<1$.

Fig. 8 Map of upper-half z plane (contour Γ) onto the D plane (contour Γ') for $s>1$.

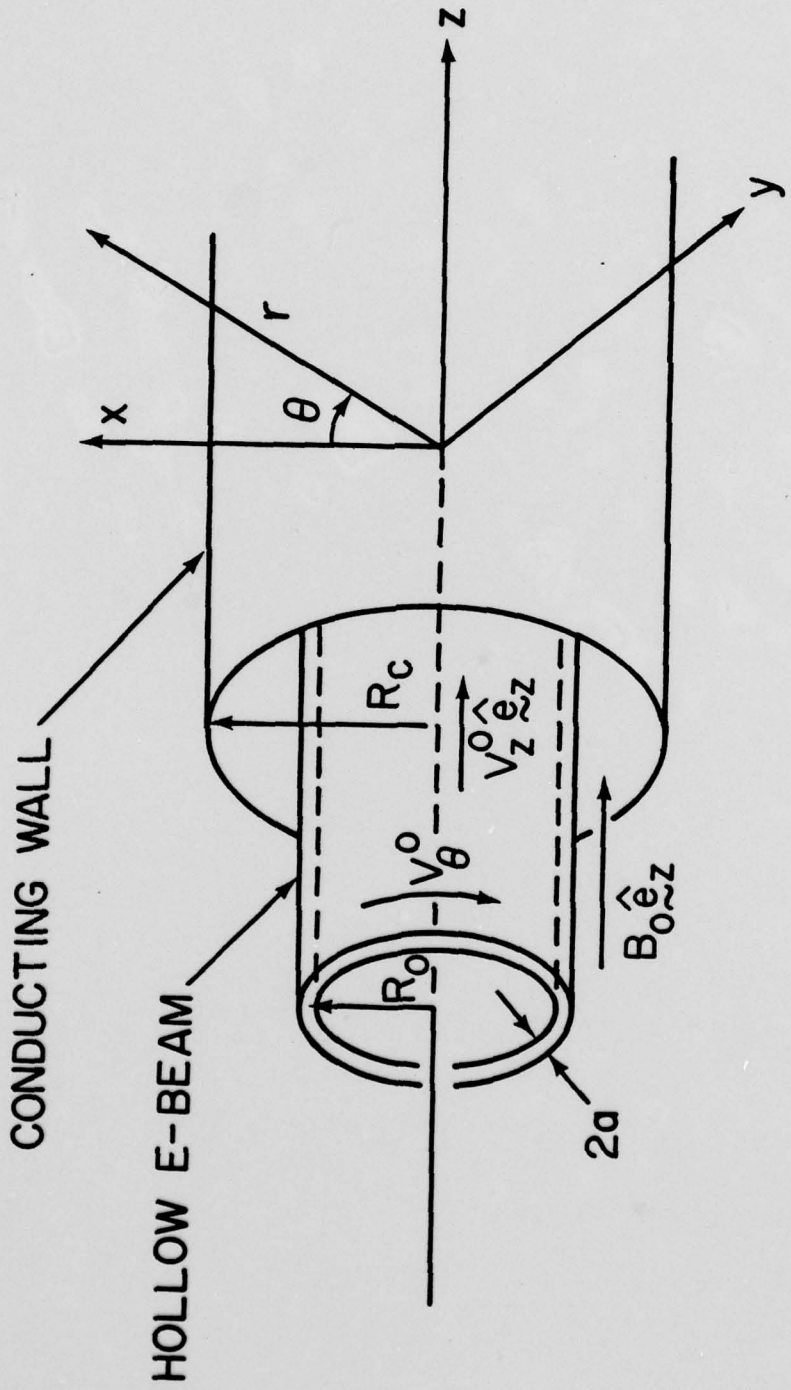
CONDUCTING WALL
HOLLOW E-BEAM
z
y
x
r
θ
R_c
R_0
V_θ^0
$V_z^0 \hat{e}_z$
$B_0 \hat{e}_z$
2a

Fig. 1

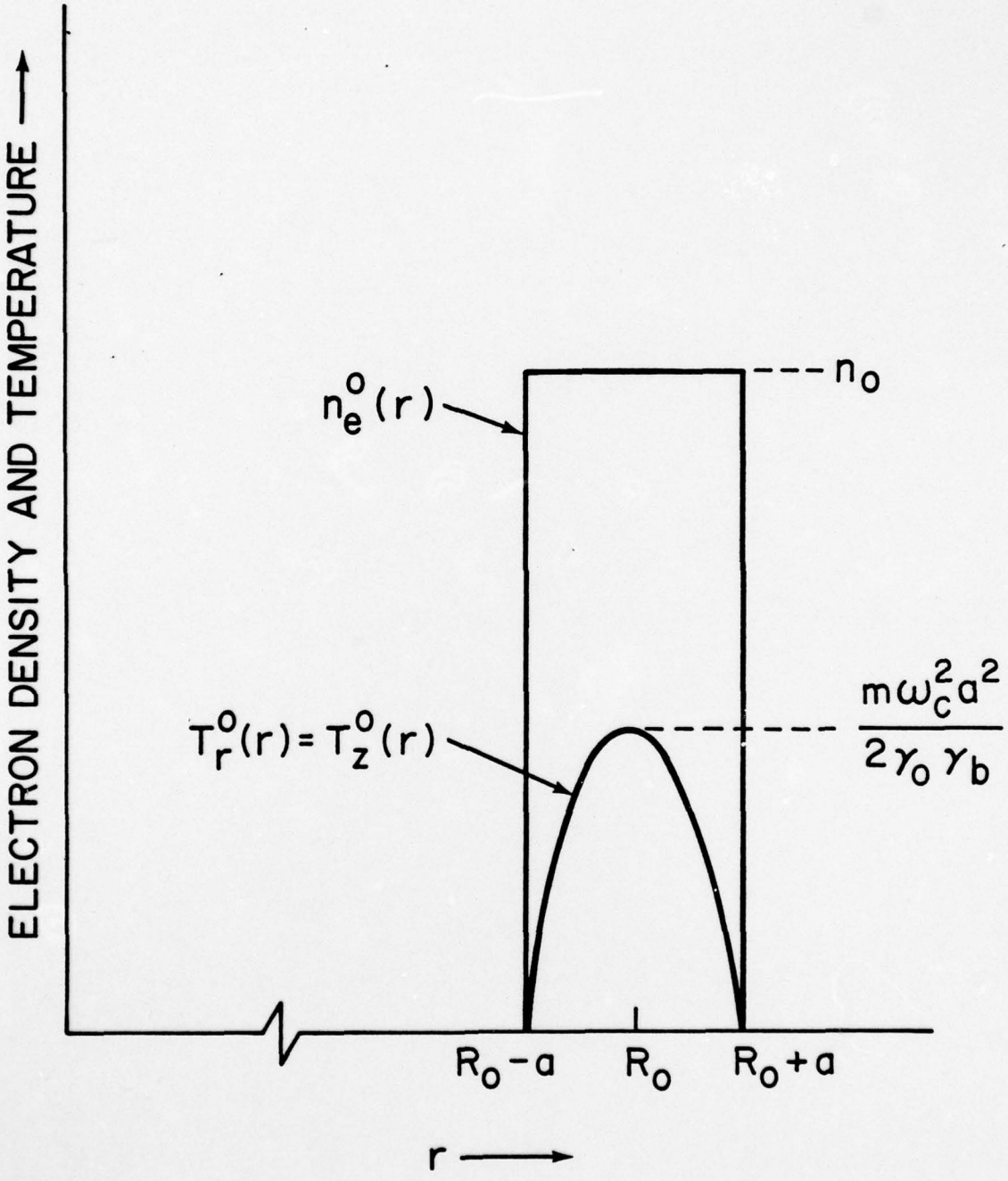
ELECTRON DENSITY AND TEMPERATURE
$n_e^o(r)$
n_o
$T_r^o(r) = T_z^o(r)$
$\frac{m\omega_c^2 a^2}{2\gamma_o \gamma_b}$
$R_o - a$
R_o
$R_o + a$
r

Fig. 2

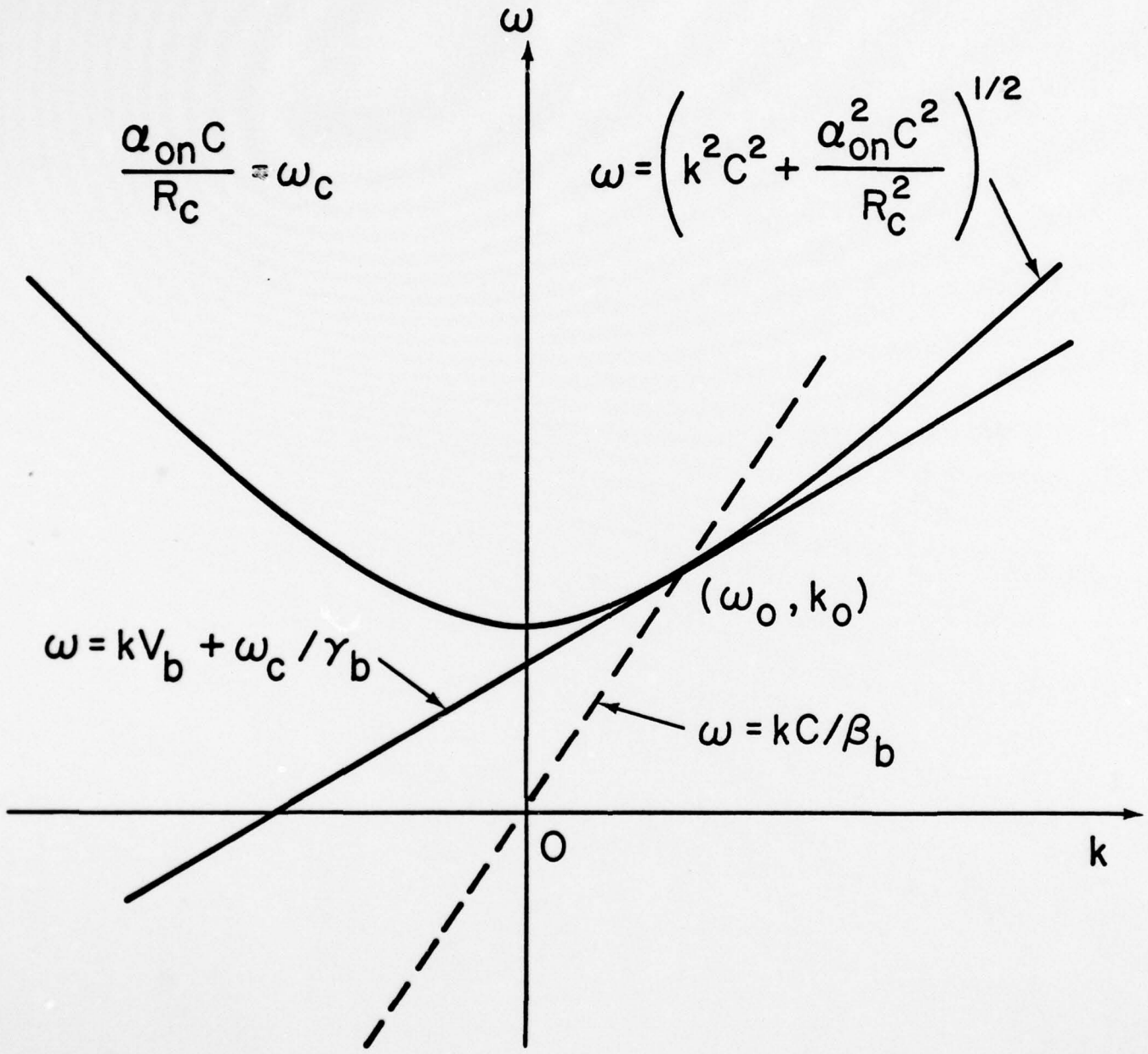
ω
$\frac{\alpha_{on}C}{R_c} = \omega_c$
$\omega = \left(k^2C^2 + \frac{\alpha_{on}^2C^2}{R_c^2}\right)^{1/2}$
(ω_o, k_o)
$\omega = kV_b + \omega_c/\gamma_b$
$\omega = kC/\beta_b$
O
k

Fig. 3

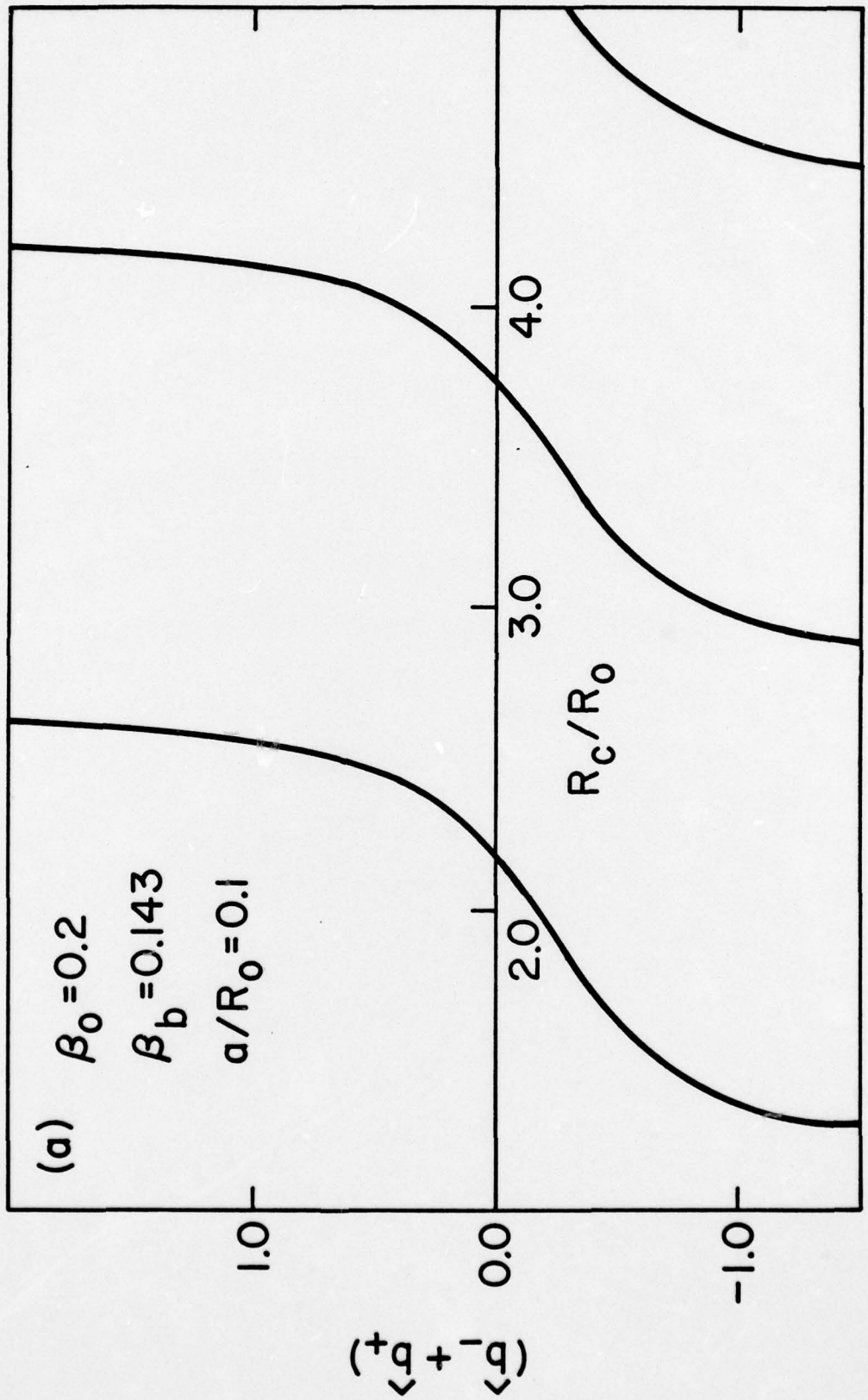

Fig. 4a

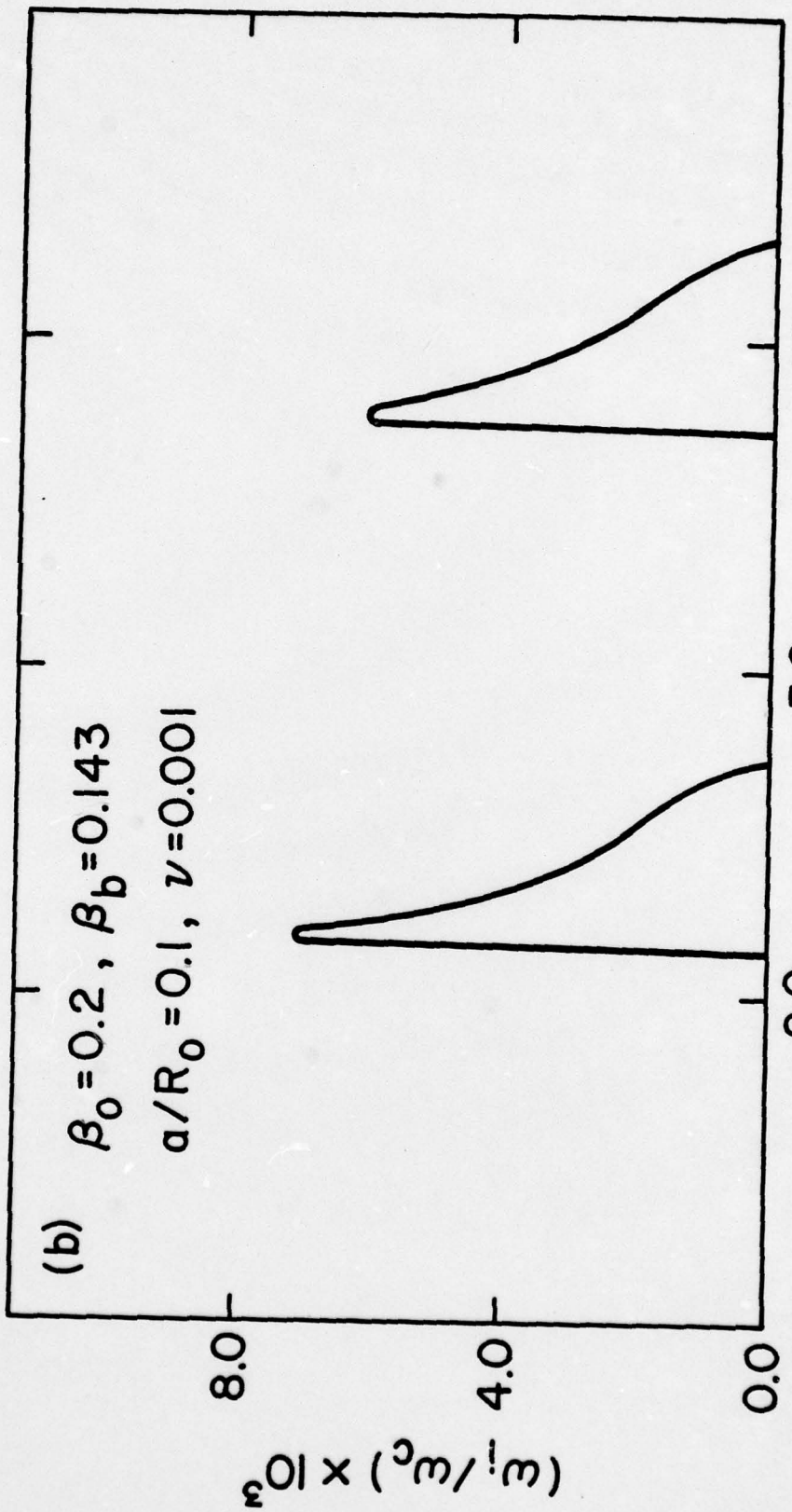
(b) β_o=0.2, β_b=0.143
a/R_o=0.1, ν=0.001
$(\omega_i/\omega_c) \times 10^3$
8.0
4.0
0.0
2.0
3.0
4.0
R_c/R_o

Fig. 4b

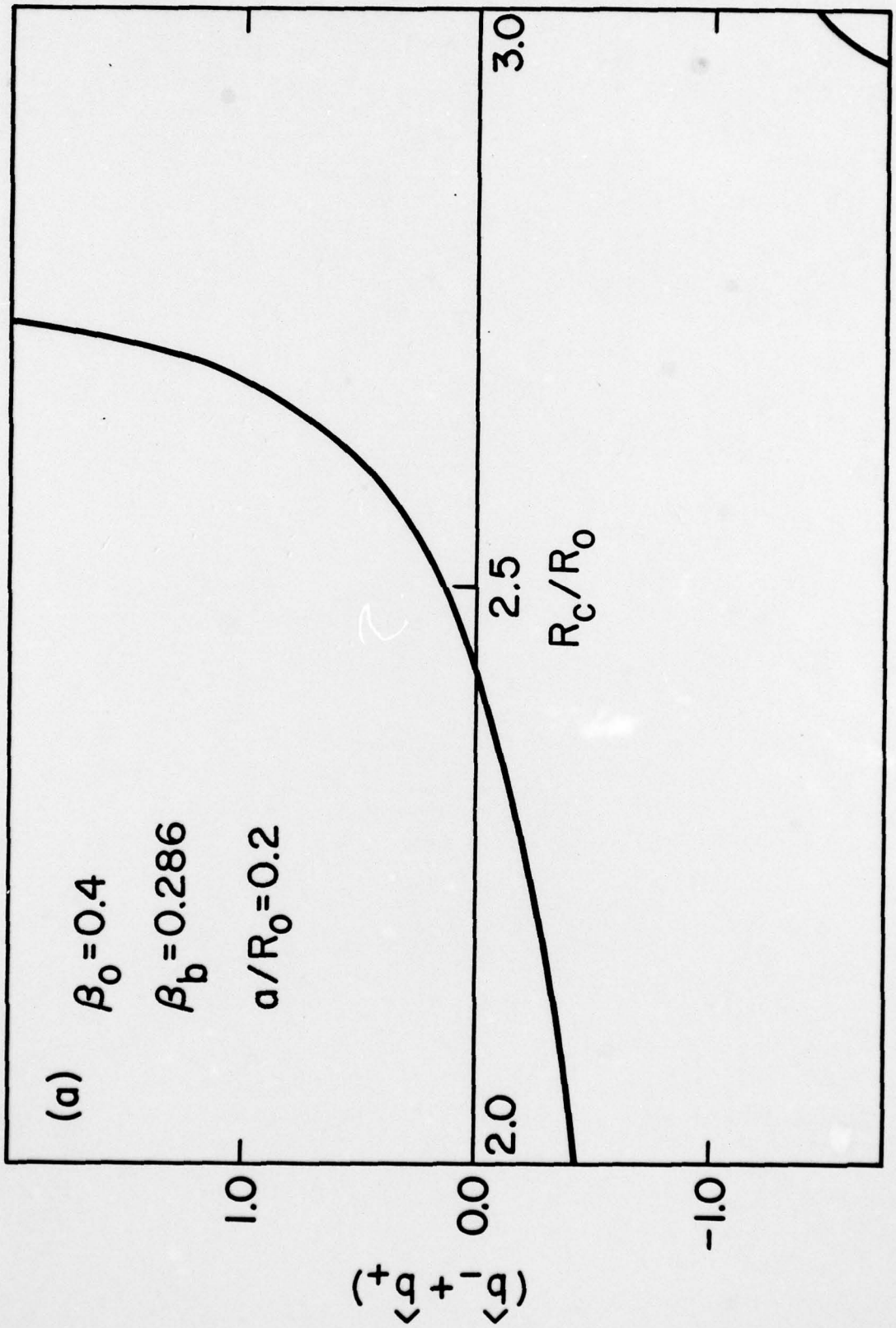

Fig. 5a

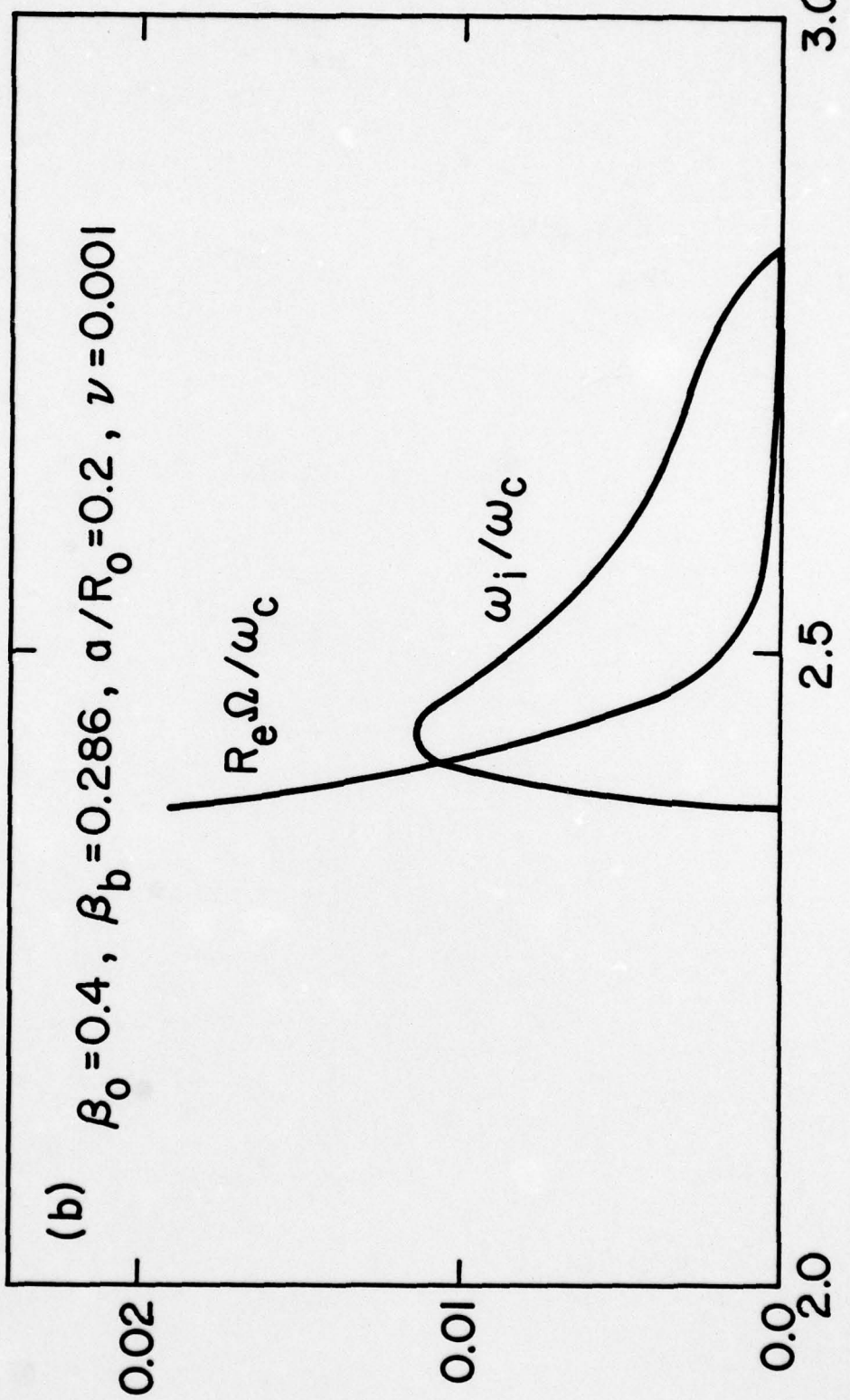
(b) β_o=0.4, β_b=0.286, a/R_o=0.2, ν=0.001
$R_e\Omega/\omega_c$
ω_i/ω_c
0.02
0.01
0.0
2.0
2.5
3.0

Fig. 5b

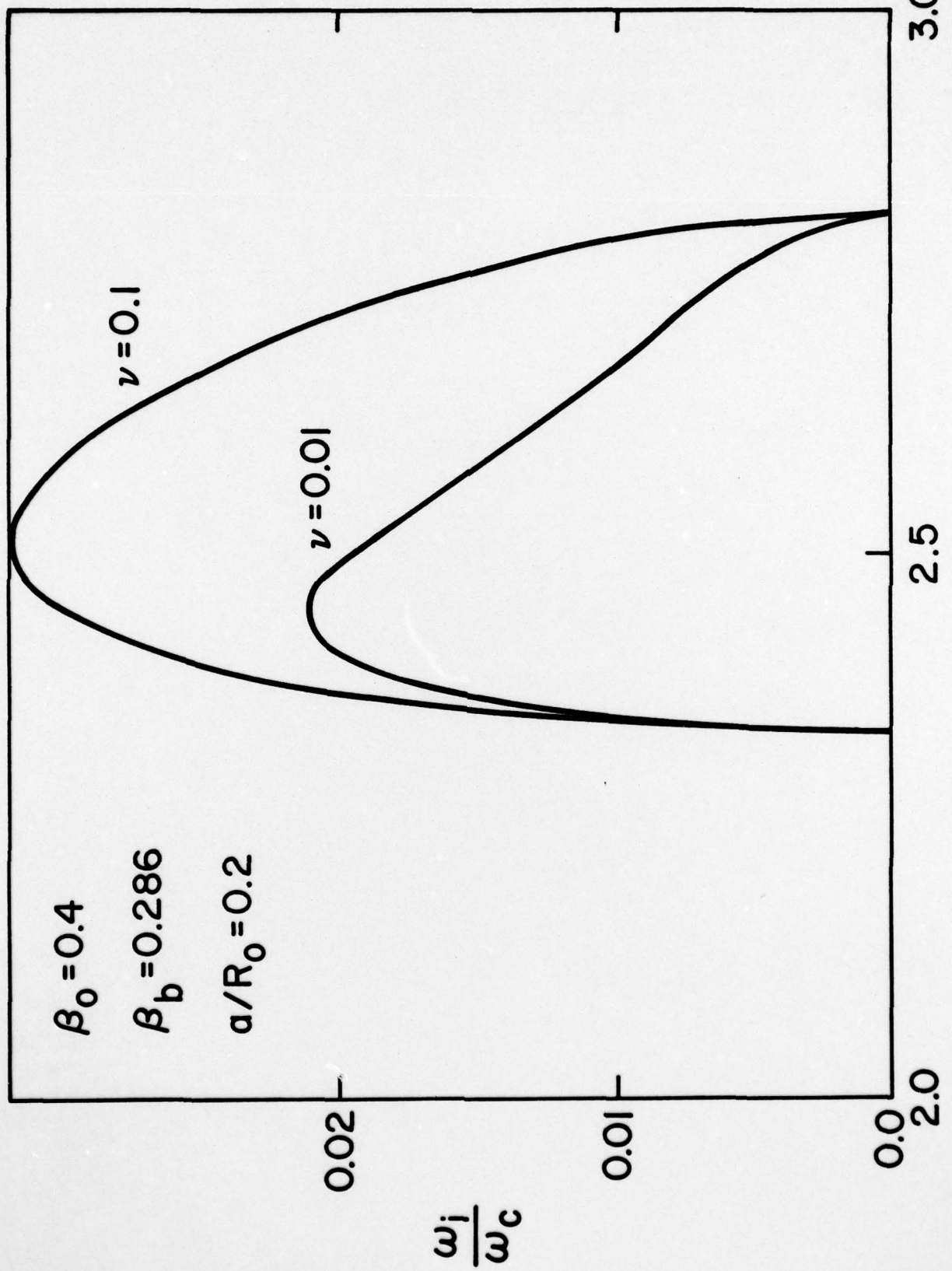
β_o=0.4
β_b=0.286
a/R_o=0.2
ν=0.1
ν=0.01
$\frac{\omega_i}{\omega_c}$
0.02
0.01
0.0
2.0
2.5
3.0
R_c/R_o

Fig. 6

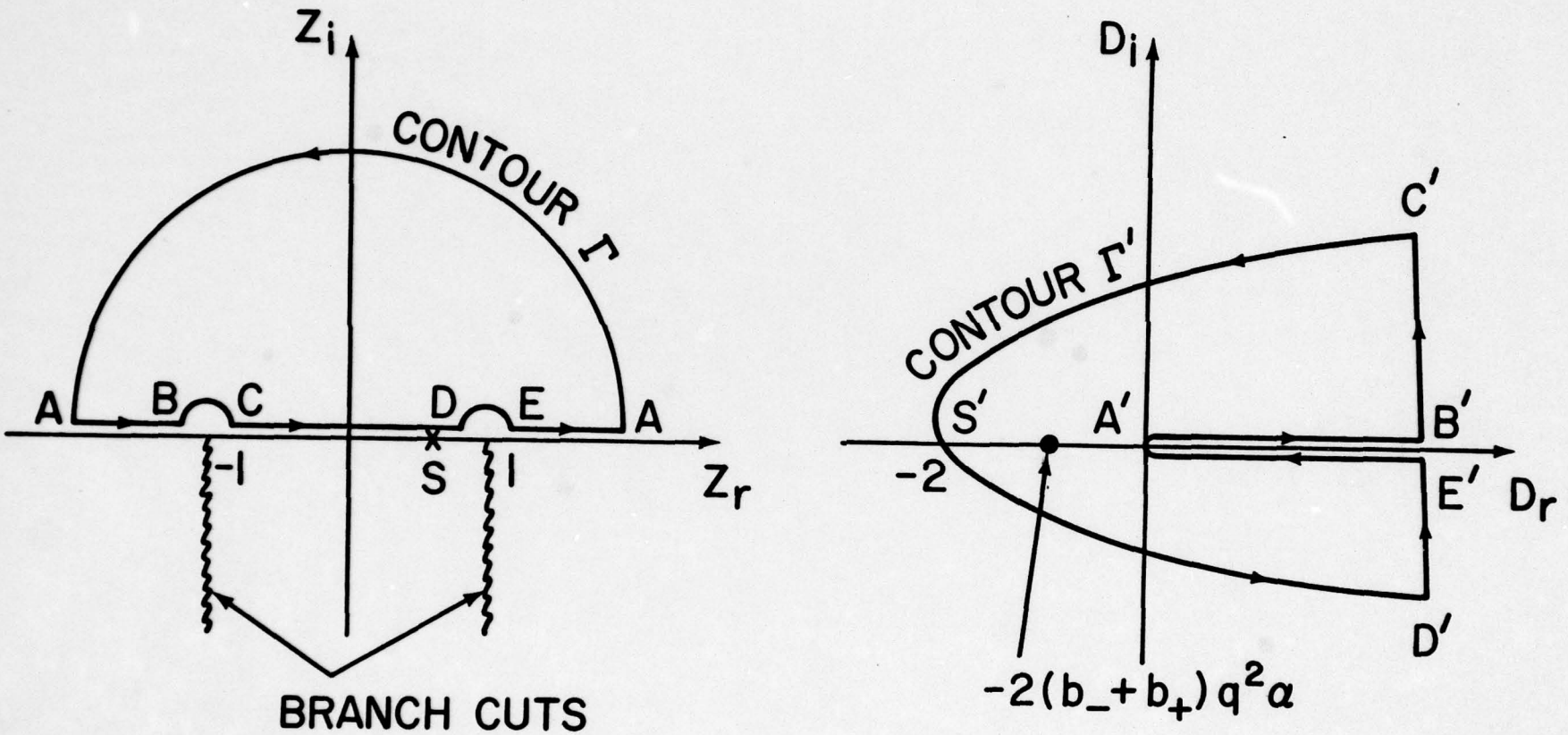
(a) Z PLANE, S<1
Z_i
CONTOUR Γ
A
B
C
D
E
A
-1
S
1
Z_r
BRANCH CUTS
(b) D PLANE, S<1
D_i
C′
CONTOUR Γ′
S′
A′
B′
-2
E′
D_r
D′
$-2(b_-+b_+)q^2\alpha$

Fig. 7

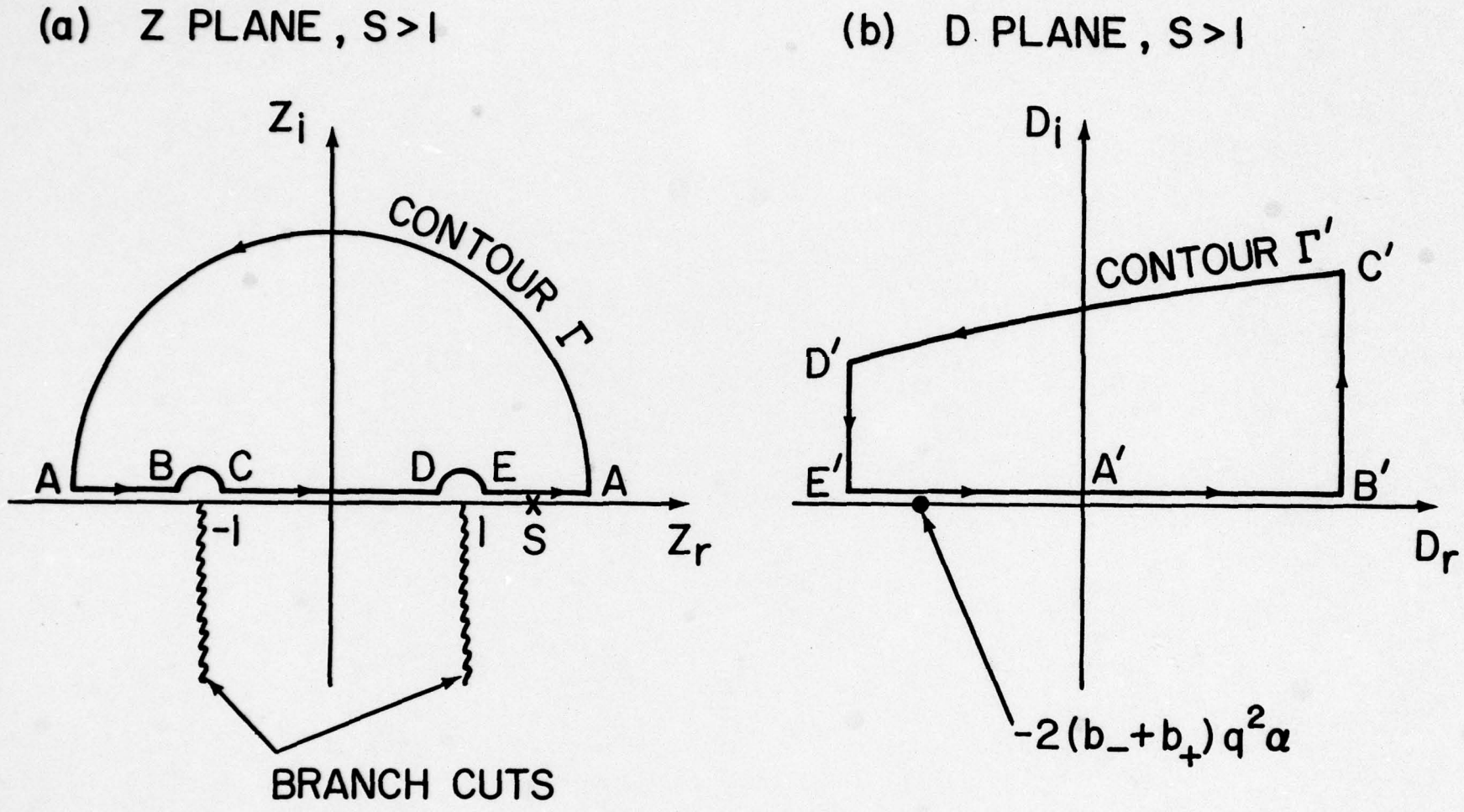
(a) Z PLANE, S>1
Z_i
CONTOUR Γ
A
B
C
D
E
A
-1
1
S
Z_r
BRANCH CUTS
(b) D PLANE, S>1
D_i
CONTOUR Γ′
C′
D′
E′
A′
B′
D_r
$-2(b_-+b_+)q^2\alpha$

Fig. 8